Nonparametric reconstruction of interaction in the cosmic dark sector

Purba Mukherjee[*] and Narayan Banerjee[†]

Department of Physical Sciences, Indian Institute of Science Education and Research Kolkata, Mohanpur, West Bengal-741246, India

(Received 16 April 2021; accepted 19 May 2021; published 11 June 2021)

The possibility of a nongravitational interaction between dark matter and dark energy is reconstructed using some recent data sets. The crucial aspect is that the interaction is not parametrized at the outset, but rather reconstructed directly from the data in a nonparametric way. The cosmic chronometer Hubble data, the Pantheon supernova compilation of CANDELS and CLASH Multi-Cycle Treasury programs obtained by the Hubble Space Telescope, and the baryon acoustic oscillation Hubble data are considered in this work. The widely accepted Gaussian process is used for the reconstruction. The results clearly indicate that a no-interaction scenario is definitely a possibility. Also, the interaction (if any) is not really significant at the present epoch. The direction of the flow of energy is clearly from dark energy to dark matter, which is consistent with the thermodynamic requirement.

DOI: 10.1103/PhysRevD.103.123530

I. INTRODUCTION

That the Universe is expanding in an accelerated fashion is now believed to be a certainty. Even though indications of this started pouring in more than 20 years ago [1,2], there is still no unequivocally accepted theoretical framework that can settle this puzzle. Surely the good old cosmological constant Λ, the "weight of the vacuum" as described by Padmanabhan, can resolve the issue [3], but it has its own share of problems, such as the enormous mismatch between the theoretically predicted value and observationally required one. This discrepancy was quite elaborately discussed in the reviews [3,4]. Various inconsistencies with Λ were in fact known even before its requirement as dark energy, the driver of the acceleration of the Universe. An account of this can be found in the famous work of Weinberg [5].

As the easiest choice of Λ as the "dark energy" runs into trouble, many other alternative models were suggested, starting from the introduction of exotic fields of various forms in the energy distribution in the realm of general relativity (GR), to different kinds of modifications of GR as the theory of gravity. For a recent review, we refer to the work of Brax [6].

In various dark energy models, the normal practice is to assume that the exotic dark energy and familiar cold dark matter evolve independently of each other. For early reviews, we refer to Refs. [3,7,8]. However, the so-called coincidence problem [9], which poses the question of why the dark energy and dark matter densities are of the same order of magnitude at the present epoch, inspired a search for any nongravitational interaction between them. In fact, a possible interaction between the vacuum energy and pressureless matter was suggested long ago; we refer, for example, to the investigations by Henriksen [10] and Olson and Jordan [11].

In the context of the present acceleration of the Universe, the idea is that dark matter and dark energy may not evolve independently; rather, there is a transfer of energy between them. As a result, they do not satisfy individual conservation equations and only the total energy is conserved via the equation $\nabla_\mu(T^{\mu\nu}_m + T^{\mu\nu}_D) = 0$, where $T^{\mu\nu}_m$ and $T^{\mu\nu}_D$ denote the energy-momentum tensors for dark matter and dark energy, respectively. A number of investigations in this direction have already been carried out, e.g., Refs. [12–21]. A function Q is introduced such that $\nabla_\mu T^{\mu\nu}_m = -\nabla_\mu T^{\mu\nu}_D \propto Q$. The function Q clearly determines the rate of transfer of energy from one sector to the other. As the origin and nature of the nongravitational interaction is not known, Q is phenomenologically chosen in various forms. Usually it is assumed to be proportional to the Hubble parameter H and the density of dark matter or dark energy. More general forms, where a linear combination of both densities or even their derivatives are involved, can also be found in the literature. For various choices and their consequences in the context of observations, we refer to Refs. [22–42]. It was shown that the interacting scenario can also potentially take care of the issues connected to the local value of the Hubble parameter [34,41,43]. For an exhaustive review, the work of Wang *et al.* is quite useful [44].

A reconstruction of the interaction from observations normally depends on the parametric form of Q, and the parameters are estimated from data sets. Another approach

[*]pm14ip011@iiserkol.ac.in
[†]narayan@iiserkol.ac.in

for reconstruction is the nonparametric one where no particular functional form of Q is assumed. Rather, one makes an attempt to ascertain the quantity directly from data, which is clearly less biased. The nonparametric approach has found many applications in cosmology. It all started with the reconstruction of physical quantities like the equation-of-state parameter of dark energy, the scalar potential when a quintessence scalar field is used as dark energy, etc. [45–52]. Recently, the nonparametric approach has been used in the reconstruction of kinematical quantities, like the deceleration parameter q [53–60] and the jerk parameter j [61].

Given that there is no *a priori* reason to rule out an interaction in the dark sector on the one hand, and the lack of any compulsive theoretical model for it on the other, certainly a reconstruction of the interaction Q, in an unbiased way without assuming any functional form of Q, deserves a lot more attention than what is available in the literature. Cai and Su [18] investigated a possible interaction, in a way independent of any specific form, by dividing the whole redshift range into a few bins and setting the interaction term to a constant in each redshift bin. The result indicated that there could be an oscillatory interaction. Wang *et al.* [62] adopted a nonparametric Bayesian approach, and indicated that an interacting vacuum is not preferred over the standard ΛCDM.

Yang *et al.* [63] presented a nonparametric reconstruction of the interaction between dark energy and dark matter directly from type Ia supernova (SNIa) Union 2.1 data using the Gaussian process. They found that unless the equation of state (EoS) parameter w for the dark energy deviates significantly from -1, the interaction is not evident. If w is very different from -1, the interaction cannot be ruled out at the 95% confidence level. A recent analysis by Cai *et al.* [64] (another nonparametric reconstruction using the Gaussian process) indicated a very interesting possibility that a gravitational-wave signal might carry signatures of the interaction in the dark sector encoded in the wave signal. That work was based on the LISA space-based interferometer. It was shown that a 10 year survey could unveil the interaction in a wide redshift domain between $1 < z < 10$.

The motivation of this work is to undertake a nonparametric reconstruction of the interaction term Q as a function of the redshift z using recent cosmological data sets. The cosmic chronometer Hubble data, the Pantheon supernova compilation of the CANDELS and CLASH Multi-Cycle Treasury programs obtained by the Hubble Space Telescope (HST), and the baryon acoustic oscillation Hubble data are utilized for this purpose. The method adopted is the widely used Gaussian process. We consider three cases for the dark energy EoS: the decaying vacuum energy Λ with $w = -1$, the wCDM model, and the Chevallier-Polarski-Linder (CPL) parametrization [65] of dark energy. Here w is the EoS parameter. For different combinations of data sets and for different choices of dark energy, the most important common feature found is that "no interaction" is almost always included at 2σ and definitely at 3σ. Also, at the present epoch an interaction is hardly indicated. Even if there's any, that would have been in the past, close to or beyond $z \sim 0.5$.

This manuscript is organized as follows. In Sec. II we describe the model with an interaction in the dark sector. Section III deals with the results of the actual reconstruction following a brief description of the Gaussian process, a summary of the data sets utilized, and the methodology. Fitting functions for the reconstructed interaction are shown in Sec. IV for different combinations of data sets. A discussion on the evolution of the density parameters is provided in Sec. V. In Sec. VI we attempt to test the reconstructed model against the laws of thermodynamics. In the last section we discuss the results obtained and make some concluding remarks.

II. THE MODEL

The infinitesimal distance element in a spatially flat, homogeneous, and isotropic universe is given by the Friedmann-Lemaître-Robertson-Walker (FLRW) metric

$$ds^2 = -c^2dt^2 + a^2(t)(dr^2 + r^2d\theta^2 + r^2\sin^2\theta d\phi^2), \quad (1)$$

where $a(t)$ is the scale factor.

The Hubble parameter, defined as the expansion rate of the universe, is given by

$$H = \frac{\dot{a}}{a}, \quad (2)$$

where a dot signifies a derivative with respect to the cosmic time t. This expression can again be written as a function of the redshift z, given by the relation $1 + z = \frac{a_0}{a}$, where any subscript 0 indicates the present value of the quantity considered and a_0 is taken to be unity. We define the dimensionless Hubble parameter as

$$E(z) = \frac{H(z)}{H_0}. \quad (3)$$

In a flat universe with an interaction between dark energy and dark matter, the Einstein equations describing the evolution of the universe are given by

$$H^2 = \frac{8\pi G}{3}(\rho_m + \rho_D), \quad (4)$$

$$\dot{H} + H^2 = -\frac{8\pi G}{6}(\rho_m + \rho_D + 3p_D), \quad (5)$$

where ρ_m denotes the energy density of dark matter, ρ_D is the energy density of the dark energy component, and we consider $8\pi G = 1$; p_D signifies the pressure component

from the dark energy sector, and $p_m = 0$ for pressureless dust. The energy conservation equation is given by the contracted Bianchi identity,

$$\dot{\rho} + 3H(1 + w_{\text{eff}})\rho = 0, \tag{6}$$

where the total energy density is given by $\rho = (\rho_m + \rho_D)$ and w_{eff} is the effective equation of state, defined as

$$w_{\text{eff}} = \frac{p}{\rho} = \frac{p_D}{\rho_m + \rho_D}. \tag{7}$$

However, this conservation equation can be separated into two parts:

$$\dot{\rho_m} + 3H\rho_m = -Q, \tag{8}$$

$$\dot{\rho_D} + 3H(1 + w)\rho_D = Q, \tag{9}$$

where $w = \frac{p_D}{\rho_D}$ is the equation of state of dark energy (DE) and Q describes the rate of transfer of energy between dark matter and dark energy. When $Q = 0$ and $w = -1$, one recovers the standard ΛCDM model. Unlike the usual practice of parametrizing the interaction term Q using any parametric form proportional to $H\rho$, here we want to reconstruct it directly from observational data using a nonparametric method.

By using $\frac{d}{dt} \equiv -H(1 + z)\frac{d}{dz}$, one can rewrite the conservation equations, with the redshift z as the argument, in the form

$$-H(1 + z)\rho'_m + 3H\rho_m = -Q(z), \tag{10}$$

$$-H(1 + z)\rho'_D + 3H(1 + w)\rho_D = Q(z). \tag{11}$$

Equation (4) can be written in terms of the dimensionless Hubble parameter $E = \frac{H}{H_0}$ as

$$E^2(z) = \tilde{\rho}_m + \tilde{\rho}_D, \tag{12}$$

where $\tilde{\rho}_m$ and $\tilde{\rho}_D$ are ρ_m and ρ_D scaled by a factor of $\frac{1}{3H_0^2}$, respectively. Upon differentiating Eq. (12) with respect to z, we get

$$2EE'(z) = \tilde{\rho}'_m + \tilde{\rho}'_D. \tag{13}$$

The conservation equations (10) can be reduced to the following forms:

$$-E(1 + z)\tilde{\rho}'_m + 3E\tilde{\rho}_m = -\tilde{Q}(z), \tag{14}$$

$$-E(1 + z)\tilde{\rho}'_D + 3E(1 + w)\tilde{\rho}_D = \tilde{Q}(z). \tag{15}$$

The dimensionless $\tilde{Q}$ characterizes the interaction, where $\tilde{Q} = \frac{1}{3H_0^3}Q$.

By combining Eq. (13) with Eqs. (14)–(15), one can obtain

$$\begin{aligned}\tilde{Q} = &\left(\frac{E^2(1 + w)}{w} + \frac{(1 + z)E^2w'}{3w^2}\right) \\ &\times [2(1 + z)E' - 3E] - \frac{(1 + z)E}{3w} \\ &\times [2(1 + z)(E'^2 + EE'') - 4EE'].\end{aligned} \tag{16}$$

From this, we see that by using the observed dimensionless Hubble parameter $E(z)$, one can reconstruct the interaction once the equation of state $w(z)$ of dark energy is known. This will be the key equation for the reconstruction of $\tilde{Q}$.

III. THE RECONSTRUCTION

To reconstruct the interaction using current data sets, we need a model-independent method to reconstruct $E(z)$, and its derivatives $E'(z)$ and $E''(z)$. In this work we use the Gaussian processes (GP) [66–68] as a numerical tool for this reconstruction purpose.

A. Gaussian process

A GP involves an indexed collection of random variables having a multivariate normal distribution. GPs can be used to infer a distribution over functions directly. The distribution of a GP is the joint distribution of all random variables, which is a distribution over functions within a continuous domain. For a given set of Gaussian-distributed observational data, we use GPs to reconstruct the most probable underlying continuous function describing that data, along with its higher derivatives, and also obtain the associated confidence levels, without limiting to any particular parametrization ansatz.

Due to its model-independent nature, this method has been widely applied in cosmology. A nonparametric reconstruction using GPs was utilized in Refs. [47–49,53–61,63,64,69–75]. We refer to the publicly available GP website [76] for more details on the method.

Let us consider a function f formed from a GP. The value of f when evaluated at a redshift point z is a Gaussian random variable with mean $\mu(z)$ and variance $\text{var}(z)$. The function value at redshift z is not independent of the function value at some other point $\tilde{z}$ (especially when z and $\tilde{z}$ are close to each other), but is related by a covariance function $\text{cov}(f(z), f(\tilde{z})) = \kappa(z, \tilde{z})$ which correlates the values of different $f(z)$ at data points z and $\tilde{z}$ separated by $|z - \tilde{z}|$ distance units.

Thus, the distribution of functions can be described by the following quantities:

$$\mu(z) = \mathcal{E}[f(z)], \tag{17}$$

$$\kappa(z, \tilde{z}) = \mathcal{E}[(f(z) - \mu(z))(f(\tilde{z}) - \mu(\tilde{z}))], \tag{18}$$

$$\mathrm{var}(z) = \kappa(z, z), \tag{19}$$

where $\mathcal{E}$ denotes the expectation.

The Gaussian process is written as

$$f(x) \sim \mathcal{GP}(\mu(z), \kappa(z, \tilde{z})), \tag{20}$$

where $\mathcal{GP}$ represents a Gaussian process.

The covariance function $\kappa(z, \tilde{z})$ depends on a set of free parameters, called the *hyperparameters*, namely, the characteristic length scale l and the signal variance σ_f. A wide range of possible covariance functions is already present in the literature [66–68]. As a standard choice one may consider the squared exponential covariance,

$$\kappa(z, \tilde{z}) = \sigma_f^2 \exp\left(-\frac{(z-\tilde{z})^2}{2l^2}\right). \tag{21}$$

Another possible choice is the Matérn covariance,

$$\kappa_{\nu=p+\frac{1}{2}}(z, \tilde{z}) = \sigma_f^2 \exp\left(\frac{-\sqrt{2p+1}}{l}|z-\tilde{z}|\right) \times \frac{p!}{(2p)!}\sum_{i=0}^{p}\frac{(p+i)!}{i!(p-i)!}\left(\frac{2\sqrt{2p+1}}{l}|z-\tilde{z}|\right)^{p-i}. \tag{22}$$

Given a data set $\mathcal{D}$ of n observations, $\mathcal{D} = \{(z_i, y_i)|_{i=1,\ldots,n}\}$, we attempt to reconstruct a function $f(z)$ that describes this data. For GPs, any z_i is assigned a random variable $f(z_i)$, and the joint distribution of a finite number of these variables $\{f(z_1), \ldots, f(z_n)\}$ is itself Gaussian,

$$\mathbf{f} \sim \mathcal{GP}(\boldsymbol{\mu}, \mathbf{K}). \tag{23}$$

For a set of input points $\mathbf{X} = \{z_i\}$, the covariance matrix $\mathbf{K} = \kappa(\mathbf{X}, \mathbf{X})$ is given by $[\kappa(\mathbf{X}, \mathbf{X})]_{ij} = \kappa(z_i, z_j)$. Here, $\boldsymbol{\mu} = (\mu(z_1), \ldots, \mu(z_n))$ and $\mathbf{f} = (f(z_1), \ldots, f(z_n))$. Excluding observational data, we use the covariance matrix $\mathbf{K}$ to generate a Gaussian vector $\mathbf{f}^*$ of function values at $\mathbf{X}^*$ with $f_i^* = f(z_i^*)$ such that

$$\mathbf{f}^* \sim \mathcal{GP}(\boldsymbol{\mu}^*, \mathbf{K}^{**}), \tag{24}$$

where $\boldsymbol{\mu}^*$ is the *a priori* assumed mean of $\mathbf{f}^*$, and $\mathbf{K}^{**} = \kappa(\mathbf{X}^*, \mathbf{X}^*)$.

Observational data (z_i, y_i) can also be described by GPs upon assuming that their errors are Gaussian. The actual observations are assumed to be scattered around the underlying function, i.e., $y_i = f(x_i) + \epsilon_i$, where Gaussian noise ϵ_i with variance σ_i^2 is assumed. This variance needs to be added to the covariance matrix,

$$\mathbf{y} \sim \mathcal{GP}(\boldsymbol{\mu}, \mathbf{K} + \mathbf{C}), \tag{25}$$

where $\mathbf{C}$ is the covariance matrix of the data. For uncorrelated data, we use $\mathbf{C} = \sigma_i^2\mathbf{I}$. The above two GPs [Eq. (24) for $\mathbf{f}^*$ and Eq. (25) for $\mathbf{y}$] can be combined in the joint distribution,

$$\begin{bmatrix}\mathbf{y}\\ \mathbf{f}^*\end{bmatrix} \sim \mathcal{GP}\left(\begin{bmatrix}\boldsymbol{\mu}\\ \boldsymbol{\mu}^*\end{bmatrix}\begin{bmatrix}\mathbf{K}+\mathbf{C} & \mathbf{K}^*\\ \mathbf{K}^{*\mathrm{T}} & \mathbf{K}^{**}\end{bmatrix}\right), \tag{26}$$

where $\mathbf{K}^* = \kappa(\mathbf{X}, \mathbf{X}^*)$ and $\mathbf{K}^{*\mathrm{T}} = \kappa(\mathbf{X}^*, \mathbf{X})$. While $\mathbf{y}$ is known from observations, we want to reconstruct $\mathbf{f}^*$.

Using standard rules for conditioning Gaussians, the predictive distribution is given by

$$\mathbf{f}^*|\mathbf{X}^*, \mathbf{X}, \mathbf{y} \sim \mathcal{GP}(\bar{\boldsymbol{\mu}}^*, \boldsymbol{\Sigma}^*), \tag{27}$$

where

$$\bar{\boldsymbol{\mu}}^* = \boldsymbol{\mu}^* + \mathbf{K}^{*\mathrm{T}}[\mathbf{K}+\mathbf{C}]^{-1}(\mathbf{y}-\boldsymbol{\mu}) \tag{28}$$

and

$$\boldsymbol{\Sigma}^* = \mathbf{K}^{**} - \mathbf{K}^{*\mathrm{T}}[\mathbf{K}+\mathbf{C}]^{-1}\mathbf{K}^* \tag{29}$$

are the mean and covariance of $\mathbf{f}^*$, respectively. Equation (27) is the posterior distribution of the function given the data (25) and the prior (24).

Although Eq. (27) covers noise in training data, it is still a distribution over noise-free predictions $\mathbf{f}$. To include noise $\boldsymbol{\epsilon}$ in the predictions $\mathbf{y}$ we add σ_i^2 to the diagonal of $\boldsymbol{\Sigma}^*$, i.e.,

$$\mathbf{y}^*|\mathbf{X}^*, \mathbf{X}, \mathbf{y} \sim \mathcal{GP}(\bar{\boldsymbol{\mu}}^*, \boldsymbol{\Sigma}^* + \mathbf{C}). \tag{30}$$

To apply the above equations for reconstructing a function, we need to estimate the hyperparameters σ_f and l. They can be trained by maximizing the marginal likelihood. Note that the marginal likelihood depends only on the locations $\mathbf{X}$ of the observations and not on the points $\mathbf{X}^*$, where we want to reconstruct the function. For a Gaussian prior $\mathbf{f}|\mathbf{X}, \sigma_f, l \sim \mathcal{GP}(\boldsymbol{\mu}, \mathbf{K})$ and with $\mathbf{y}|\mathbf{f} \sim \mathcal{GP}(\mathbf{f}, \mathbf{C})$, the log marginal likelihood is given by

$$\ln\mathcal{L} = -\frac{1}{2}(\mathbf{y}-\boldsymbol{\mu})^{\mathrm{T}}[\mathbf{K}+\mathbf{C}]^{-1}(\mathbf{y}-\boldsymbol{\mu}) - \frac{1}{2}\ln|\mathbf{K}+\mathbf{C}| - \frac{n}{2}\ln 2\pi. \tag{31}$$

The hyperparameters σ_f and l are optimized by maximizing Eq. (31).

This approach also provides a robust way to estimate derivatives of the function. While the covariance between the observational points stays the same, one also needs a covariance between the function and its derivative and another between the derivatives for the reconstruction.

These covariances can be obtained by differentiating the original covariance function $\kappa(x, \tilde{x})$.

In the present work, the observational Hubble data from cosmic chronometers and baryon acoustic oscillations, along with the reduced Hubble data from the Pantheon supernova compilation of the CANDELS and CLASH Multi-Cycle Treasury programs, forms the function space. The target function is $E(z)$, and its derivatives are $E'(z)$ and $E''(z)$, which are to be reconstructed using the GP method.

We have used both the squared exponential and the Matérn $(\nu = \frac{9}{2}, p = 4)$ covariance functions. The former has the advantage of being indefinitely differentiable. The Matérn function (ν) leads to reliable and stable results when $\nu > n$ where derivatives up to nth order are required. In the present work, we need to use up to second-order derivatives, so ν is easily greater than n. For a comprehensive comparison of various covariance functions, we refer to the work of Seikel and Clarkson [77]. In contrast to actual parameters, GPs do not specify the form of the reconstructed function; rather, it characterizes the typical changes in the function. The publicly available GaPP [78] (Gaussian processes in PYTHON) code by Seikel *et al.* [69] is employed in this work.

B. Observational data sets

The background data viz. the cosmic chronometer (CC) Hubble data, the Pantheon supernova compilation of the CANDELS and CLASH Multi-Cycle Treasury (MCT) programs obtained by the HST, and the baryon acoustic oscillation (BAO) Hubble data are utilized to reconstruct the cosmic interaction as a function of redshift. A brief summary of the data sets is given below.

1. CC data

The Hubble parameter $H(z)$ is estimated by calculating the differential ages of galaxies [79–84], usually called cosmic chronometers, as

$$H(z) = -\frac{1}{1+z}\frac{dz}{dt}. \tag{32}$$

The CC data are independent of the Cepheid distance scale and do not assume any background cosmological model. However, they are subject to other sources of systematic uncertainties, such as the modeling of stellar ages carried out through the stellar population synthesis (SPS) techniques. Given a pair of ensembles of passively evolving galaxies at two different redshifts, it is possible to infer $\frac{\Delta z}{\Delta t}$ from observations under the assumption of a concrete SPS model [85–87]. Thus, $H(z)$ can be directly computed using Eq. (32), the quantity we are interested in. Therefore, the CC measurements allow us to obtain direct information about the Hubble function at different z, contrary to other probes which do not directly measure $H(z)$, but rather integrated quantities such as luminosity distances. In the present work, we use both the BC03 and MaStro11 SPS compilations of CC measurements shown in Table I including almost all $H(z)$ data reported in various surveys so far. The sources of these data sets are quoted in the table.

TABLE I. Cosmic chronometer Hubble parameter H measurements (in units of $\mathrm{km\,s^{-1}\ Mpc^{-1}}$) and their errors σ_H at redshift z obtained from the differential age method.

Index	z	$H \pm \sigma_H$ *(BC03)*	$H \pm \sigma_H$ *(MaStro11)*	References
1	0.07	69 ± 19.6	⋯	[79]
2	0.1	69 ± 12	⋯	[80]
3	0.12	68.6 ± 26.2	⋯	[79]
4	0.17	83 ± 8	⋯	[80]
5	0.1797	75 ± 4	81 ± 5	[81]
6	0.1993	75 ± 5	81 ± 6	[81]
7	0.2	72.9 ± 29.6	⋯	[79]
8	0.27	77 ± 14	⋯	[80]
9	0.28	88.8 ± 36.6	⋯	[79]
10	0.3519	83 ± 14	88 ± 16	[81]
11	0.3802	83 ± 13.5	89.2 ± 14.1	[82]
12	0.4	95 ± 17	⋯	[80]
13	0.4004	77.0 ± 10.2	82.8 ± 10.6	[82]
14	0.4247	87.1 ± 11.2	93.7 ± 11.7	[82]
15	0.4497	92.8 ± 12.9	99.7 ± 13.4	[82]
16	0.47	89 ± 34	⋯	[83]
17	0.4783	80.9 ± 9.0	86.6 ± 8.7	[82]
18	0.48	97 ± 60	⋯	[80]
19	0.5929	104 ± 13	110 ± 15	[81]
20	0.6797	92 ± 8	98 ± 10	[81]
21	0.7812	105 ± 12	88 ± 11	[81]
22	0.8754	125 ± 17	124 ± 17	[81]
23	0.88	90 ± 40	⋯	[80]
24	0.9	117 ± 23	⋯	[80]
25	1.037	154 ± 20	113 ± 15	[81]
26	1.3	168 ± 17	⋯	[80]
27	1.363	160 ± 33.6	⋯	[84]
28	1.43	177 ± 18	⋯	[80]
29	1.53	140 ± 14	⋯	[80]
30	1.75	202 ± 40	⋯	[80]
31	1.965	186.5 ± 50.4	⋯	[84]

2. Pantheon+MCT data

We make use of the Hubble rate data points, i.e., $E(z_i) = H(z_i)/H_0$ provided in Ref. [88] for six different redshifts in the range $z \in [0.07, 1.5]$ shown in Table II. They compress information very effectively about the 1048 SNIa data at $z < 1.5$, which is a part of the Pantheon compilation (which includes 740 SNIa of the joint light-curve analysis sample) and the 15 SNIa at $z > 1$ of the CANDELS and CLASH MCT programs obtained by HST, nine of which are at $1.5 < z < 2.3$. Riess *et al.* [88] converted the raw SNIa measurements into data on $E(z)$ by parametrizing $E^{-1}(z)$. The corresponding values of $E^{-1}(z_i)$ are Gaussian to a very good approximation, as shown in the work of Riess *et al.* [88] which also contains the corresponding correlation

TABLE II. $E(z)$ obtained from the inversion of $E^{-1}(z)$ data reported in Table 6 of Ref. [88]. Note the difference in the estimate of $E(z=1.5)$ from the actual quoted value. We pick up the mean value obtained from an inversion of the quoted $E^{-1}(z)$. The inverse covariance matrix has been included in our analysis.

Index	z	$E(z)$
1	0.07	0.997 ± 0.023
2	0.20	1.111 ± 0.021
3	0.35	1.127 ± 0.037
4	0.55	1.366 ± 0.062
5	0.9	1.524 ± 0.121
6	1.5	2.924 ± 0.675

matrix. Here, we have adopted the mean value obtained from the inversion of quoted $E^{-1}(z)$ and the inverse covariance matrix.

3. BAO data

An alternative compilation of the $H(z)$ data can be deduced from the radial BAO peaks in the galaxy power spectrum, or from the BAO peak using the Ly-α forest of quasi-steller objects (QSOs), which are based on the clustering of galaxies or quasars [89–102]. Table III includes almost all data reported in various surveys so far. One may find that some of the $H(z)$ data points from clustering measurements are correlated since either they belong to the same analysis or there is an overlap between the galaxy samples. We take into account all covariances among the respective data points in our analysis.

C. Methodology

We consider three choices for the dark energy equation-of-state parameter $w = \frac{p_D}{\rho_D}$. First we consider the decaying vacuum energy case, followed by the wCDM model, and finally the CPL parametrization,

$$\Lambda\text{CDM}:\ w(z) = -1, \tag{33}$$

$$w\text{CDM}:\ w(z) = w, \tag{34}$$

$$\text{CPL}:\ w(z) = w_0 + w_a\left(\frac{z}{1+z}\right). \tag{35}$$

For the dark energy EoS, considering the wCDM model, we take the best-fit value of $w = -1.006 \pm 0.045$ from the *Planck* 2015 data [103], and for the CPL parametrization $w(z) = w_0 + w_a(\frac{z}{1+z})$ we take $w_0 = -1.046^{+0.179}_{-0.170}$ and $w_a = 0.14^{+0.60}_{-0.76}$, respectively, from the HST Cluster Supernova Survey 2011 [104].

We attempt to reconstruct $\tilde{Q}$ directly through the Gaussian process for the following combination of data sets:

(1) *Set A*
   (a) CC(BC03) + Pantheon + MCT
   (b) CC(MaStro) + Pantheon + MCT

TABLE III. Hubble parameter measurements $H(z)$ (in units of $\text{kms}^{-1}\ \text{Mpc}^{-1}$) and their errors σ_H at redshift z obtained from the radial BAO method.

Index	z	$H \pm \sigma_H$	References
1	0.24	79.69 ± 2.99	[89]
2	0.3	81.7 ± 6.22	[90]
3	0.31	78.17 ± 4.74	[91]
4	0.34	83.8 ± 3.66	[89]
5	0.35	82.7 ± 8.4	[92]
6	0.36	79.93 ± 3.39	[91]
7	0.38	81.5 ± 1.9	[93]
8	0.40	82.04 ± 2.03	[91]
9	0.43	86.45 ± 3.68	[89]
10	0.44	82.6 ± 7.8	[94]
11	0.44	84.81 ± 1.83	[91]
12	0.48	87.79 ± 2.03	[91]
13	0.51	90.4 ± 1.9	[93]
14	0.52	94.35 ± 2.65	[91]
15	0.56	93.33 ± 2.32	[91]
16	0.57	87.6 ± 7.8	[96]
17	0.57	96.8 ± 3.4	[97]
18	0.59	98.48 ± 3.19	[91]
19	0.6	87.9 ± 6.1	[94]
20	0.61	97.3 ± 2.1	[93]
21	0.64	98.82 ± 2.99	[91]
22	0.73	97.3 ± 7	[94]
23	0.978	113.72 ± 14.63	[101]
24	1.23	131.44 ± 12.42	[101]
25	1.526	148.11 ± 12.71	[101]
26	1.944	172.63 ± 14.79	[101]
27	2.3	224 ± 8	[95]
28	2.33	224 ± 8	[98]
29	2.34	222 ± 7	[99]
30	2.36	226 ± 8	[100]
31	2.4	227.8 ± 5.61	[102]

(2) *Set B*
   (a) CC(BC03) + Pantheon + MCT + BAO
   (b) CC(MaStro) + Pantheon + MCT + BAO

We start with constraining the Hubble parameter in the present epoch (H_0). With the Hubble data, we utilize the GP method to reconstruct $H(z)$. The value of H_0 obtained is shown in Table IV. Further, we normalize the reconstructed data set to obtain the dimensionless or reduced Hubble parameter $E(z) = \frac{H(z)}{H_0}$. Considering the error of the Hubble constant σ_H, we can calculate the uncertainty associated with E, i.e., σ_E as

TABLE IV. Reconstructed value of H_0 using samples from Sets A and B.

$\kappa(z,\tilde{z})$	A 1	A 2	B 1	B 2
Sq. Exp	67.36 ± 4.77	72.13 ± 4.85	65.19 ± 2.63	67.66 ± 2.79
Matérn 9/2	68.47 ± 5.08	72.76 ± 5.00	65.15 ± 2.72	67.57 ± 2.90

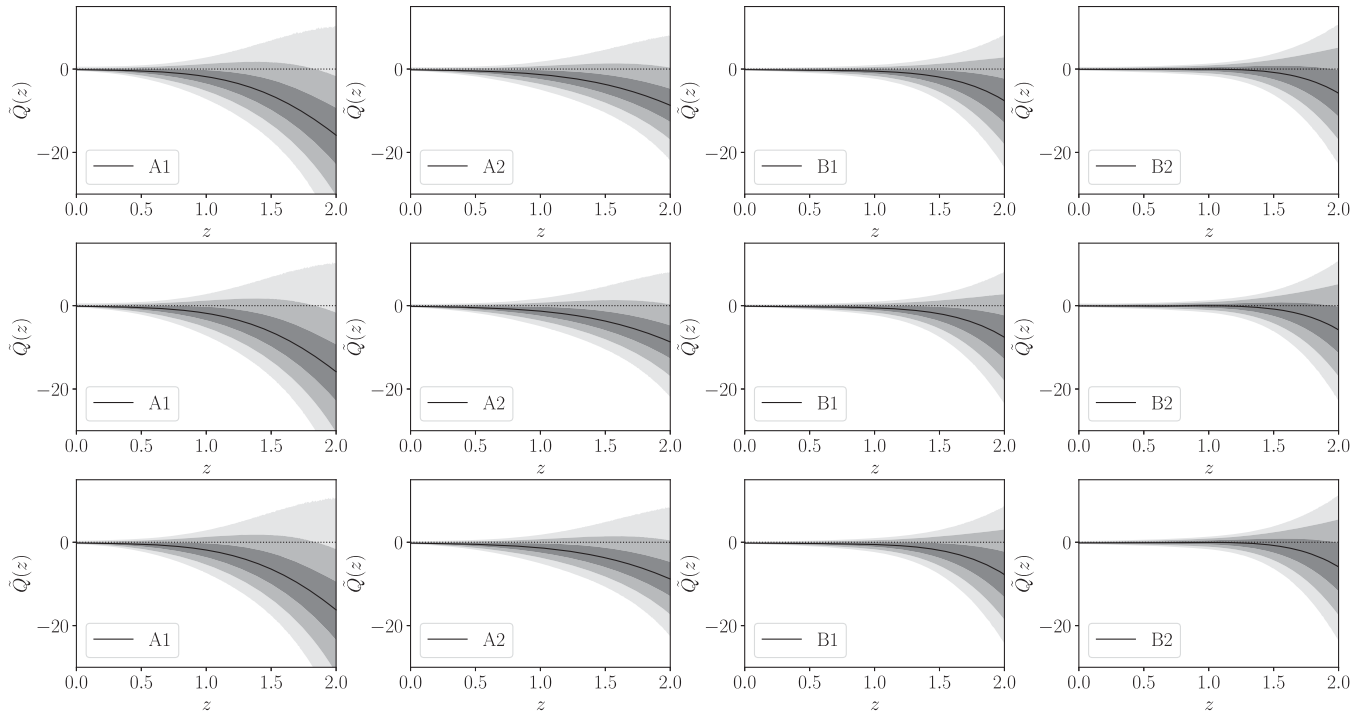

FIG. 1. Plots for the reconstructed interaction term $\tilde{Q}$ from the data set samples of Sets A and B using a squared exponential covariance function considering the decaying dark energy EoS given by $w = -1$ (top row), the wCDM model with DE EoS given by $w = -1.006 \pm 0.045$ [103] (middle row), and the CPL parametrization of dark energy with DE EoS given by $w(z) = w_0 + w_a(\frac{z}{1+z})$, $w_0 = -1.046^{+0.179}_{-0.170}$, and $w_a = 0.14^{+0.60}_{-0.76}$ [104] (bottom row). The black solid curve shows the best-fit values and the shaded regions correspond to the 1σ, 2σ, and 3σ uncertainties.

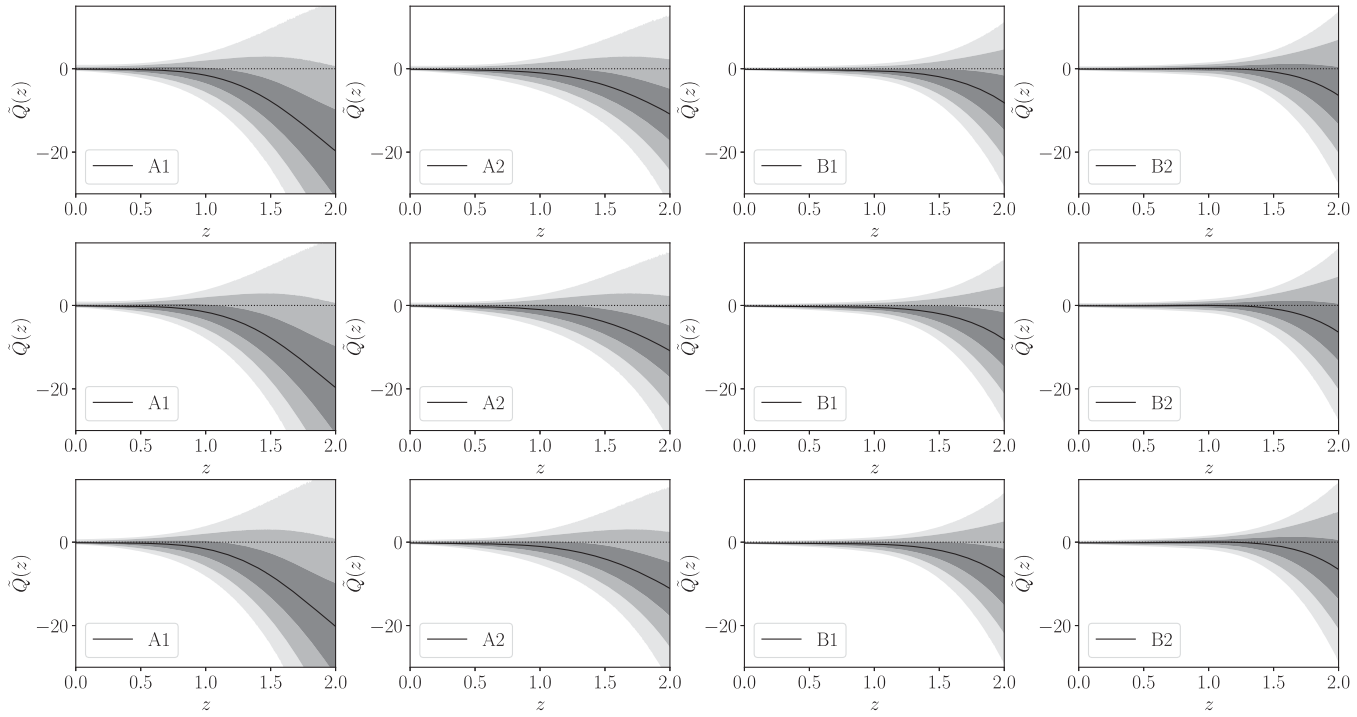

FIG. 2. Plots for the reconstructed interaction term $\tilde{Q}$ from the data set samples of Sets A and B using a Matérn 9/2 covariance function considering the decaying dark energy EoS given by $w = -1$ (top row), the wCDM model with DE EoS given by $w = -1.006 \pm 0.045$ [103] (middle row), and the CPL parametrization of dark energy with EoS given by $w(z) = w_0 + w_a(\frac{z}{1+z})$, $w_0 = -1.046^{+0.179}_{-0.170}$, and $w_a = 0.14^{+0.60}_{-0.76}$ [104] (bottom row). The black solid curve shows the best-fit values and the shaded regions correspond to the 1σ, 2σ, and 3σ uncertainties.

TABLE V. Reconstructed value of $\tilde{Q}(z=0)$ using samples from Sets A and B for the decaying dark energy EoS given by $w=-1$.

$\kappa(z,\tilde{z})$	A 1	A 2	B 1	B 2
Sq. Exp	$-0.133^{+0.126+0.343+0.686}_{-0.096-0.190-0.296}$	$-0.162^{+0.119+0.301+0.581}_{-0.088-0.170-0.261}$	$-0.129^{+0.102+0.234+0.417}_{-0.076-0.138-0.198}$	$-0.063^{+0.146+0.331+0.571}_{-0.109-0.193-0.269}$
Matérn 9/2	$-0.085^{+0.204+0.529+1.016}_{-0.145-0.280-0.429}$	$-0.127^{+0.174+0.433+0.812}_{-0.122-0.230-0.347}$	$-0.141^{+0.121+0.280+0.492}_{-0.092-0.168-0.243}$	$-0.085^{+0.168+0.381+0.671}_{-0.126-0.224-0.316}$

TABLE VI. Reconstructed value of $\tilde{Q}(z=0)$ using samples from Sets A and B for the wCDM model with EoS given by $w=-1.006\pm0.045$ [103].

$\kappa(z,\tilde{z})$	A 1	A 2	B 1	B 2
Sq. Exp	$-0.135^{+0.124+0.335+0.670}_{-0.096-0.190-0.296}$	$-0.165^{+0.116+0.296+0.567}_{-0.086-0.168-0.257}$	$-0.133^{+0.099+0.228+0.409}_{-0.075-0.136-0.197}$	$-0.069^{+0.143+0.324+0.564}_{-0.107-0.189-0.266}$
Matérn 9/2	$-0.088^{+0.202+0.518+1.008}_{-0.143-0.278-0.425}$	$-0.130^{+0.170+0.425+0.804}_{-0.120-0.229-0.345}$	$-0.146^{+0.118+0.273+0.488}_{-0.091-0.167-0.244}$	$-0.091^{+0.165+0.376+0.653}_{-0.124-0.219-0.311}$

$$\sigma_E{}^2 = \frac{\sigma_H{}^2}{H_0{}^2} + \frac{H^2}{H_0{}^4}\sigma_{H_0}{}^2, \tag{36}$$

where σ_{H_0} is the error associated with H_0.

We normalize the CC and BAO Hubble data with the reconstructed H_0 to obtain $E(=\frac{H}{H_0})$, with $E(z=0)=1$. These are now combined with E data obtained from the Pantheon + MCT compilation. The error uncertainties and the covariance matrix associated with individual data sets have been combined and taken into account. Assuming that the E data obey a Gaussian distribution with a mean and variance, the posterior distribution of the reconstructed function $E(z)$ and its derivatives can be expressed as a joint Gaussian distribution of different data sets. Thus, given a set of observational data, we have used the GP to construct the most probable underlying continuous function $E(z)$ describing the data, along with its derivatives, and have also obtained the associated confidence levels. Using the reconstructed values of $E(z)$, $E'(z)$, and $E''(z)$ in Eq. (16), the interaction $\tilde{Q}(z)$ is reconstructed.

D. Results

In the present work, we make an attempt to get an essence of how the reconstructed interaction function evolves with redshift. The motivation is to find the nature of the deviation from the zero-interaction scenario. We reconstruct the dimensionless cosmic interaction $\tilde{Q}(z)$ using the GP method for three choices of the dark energy equation-of-state parameter w. Also, two choices for the covariance function are considered. The reconstructed interaction function $\tilde{Q}$ for various combinations of data sets for each of the three dark energy models for the two choices of covariance function are shown in Figs. 1 and 2. The shaded regions correspond to the 68%, 95%, and 99.7% C.L., respectively, from darker to lighter shades. The black solid line shows the curve with the best-fit values of $\tilde{Q}$. Tables V–VII show the best-fit results for $\tilde{Q}(z=0)$ along with the 1σ, 2σ, and 3σ uncertainties for all combinations. In Figs. 3 and 4, we zoom in on the plots for $\tilde{Q}$ in the range $0<z<0.5$ to look at their behavior at very low redshift more closely. It may be noted that Figs. 1–4 are essentially plots of Eq. (16).

From Eq. (10) one can understand that a negative Q indicates an energy flow from the dark energy to the dark matter sector, and a positive Q indicates the reverse. The plots show that the interaction function $\tilde{Q}$ remains close to 0, indicating no appreciable interaction for low redshift ranges. The best-fit curve shows a small deviation towards negative values, but the zero-interaction scenario is always included at 2σ for most of the combinations. So the energy gets transferred from the dark energy to the dark matter sector, if it happens at all. This direction of the flow of energy is consistent with the thermodynamic requirement, as discussed by Pavón and Wang [105]. Interestingly, the case of $\tilde{Q}<0$ guarantees that the ratio $\frac{\rho_m}{\rho_D}$ asymptotically tends to a constant [106], and thus alleviates the coincidence problem.

IV. FITTING FUNCTION FOR $\tilde{Q}$

In this section, an approximate fitting formula for the reconstructed interaction is derived. This is done in the low redshift range $0<z<1$ using the combined data sets A1, A2, B1, and B2. The goal is to find a simple analytic form of $\tilde{Q}$ prior to the transition. As both covariance functions yield similar results, we only choose one of them, namely, the Matérn 9/2 covariance, as an example. We consider a polynomial for $\tilde{Q}(z)$ as a function of redshift z as

$$\tilde{Q}_{\rm fit}(z) = \sum_{i=0}^{n} \tilde{Q}_i z^i. \tag{37}$$

We estimate the coefficients $\tilde{Q}_i$ of the above equation using the χ^2 minimization, where we define the χ^2 function as

TABLE VII. Reconstructed value of $\tilde{Q}(z=0)$ using samples from Sets A and B for the CPL parametrization of dark energy with EoS given by $w(z) = w_0 + w_a(\frac{z}{1+z})$, $w_0 = -1.046^{+0.179}_{-0.170}$, and $w_a = 0.14^{+0.60}_{-0.76}$ [104].

$\kappa(z,\tilde{z})$	A 1	A 2	B 1	B 2
Sq. Exp	$-0.175^{+0.097+0.249+0.520}_{-0.091-0.185-0.293}$	$-0.214^{+0.087+0.217+0.429}_{-0.080-0.162-0.253}$	$-0.202^{+0.073+0.169+0.306}_{-0.061-0.117-0.177}$	$-0.159^{+0.111+0.253+0.448}_{-0.085-0.155-0.255}$
Matérn 9/2	$-0.136^{+0.157+0.410+0.814}_{-0.132-0.263-0.412}$	$-0.187^{+0.131+0.330+0.638}_{-0.108-0.214-0.331}$	$-0.213^{+0.091+0.209+0.374}_{-0.076-0.146-0.221}$	$-0.178^{+0.131+0.299+0.530}_{-0.100-0.186-0.272}$

$$\chi^2 = \sum_s \frac{[\tilde{Q}(z_s) - \tilde{Q}_{\rm fit}(z_s)]^2}{\sigma^2(z_s)}. \tag{38}$$

We perform the fitting using a trial and error estimation for different orders of i in Eq. (37). The value of the reduced χ^2, defined as $\chi^2_\nu = \frac{\chi^2}{\nu}$, where ν signifies the degrees of freedom, is estimated. This procedure entails going from order to order in the polynomial and getting the best-fitting χ^2, and truncating once χ^2_ν falls below one to prevent overfitting. Again, the estimated $\tilde{Q}_i$ along with their 1σ uncertainties are given. A comparison between the reconstructed $\tilde{Q}(z)$ and estimated $\tilde{Q}_{\rm fit}$ for various combinations of data sets are shown in Figs. 5–8. The best-fit values of the coefficients are shown in Tables VIII and IX.

For the A1 data set, in the redshift range $0 < z < 0.6$,

$$\tilde{Q}_{\rm fit}(z) = -0.060 - 0.322\,z \quad \text{for } w = -1, \tag{39}$$

$$= -0.063 - 0.324\,z \quad \text{for } w\text{CDM}, \tag{40}$$

$$= -0.114 - 0.286\,z \quad \text{for CPL}. \tag{41}$$

For the A1 data set, in the redshift range $0.6 < z < 1$,

$$\tilde{Q}_{\rm fit}(z) = 0.443 - 1.865\,z^2 \quad \text{for } w = -1, \tag{42}$$

$$= 0.438 - 1.866\,z^2 \quad \text{for } w\text{CDM}, \tag{43}$$

$$= 0.424 - 1.882\,z^2 \quad \text{for CPL}. \tag{44}$$

For the A2 data set, in the redshift range $0 < z < 0.6$,

$$\tilde{Q}_{\rm fit}(z) = -0.110 - 0.375\,z \quad \text{for } w = -1, \tag{45}$$

$$= -0.115 - 0.379\,z \quad \text{for } w\text{CDM}, \tag{46}$$

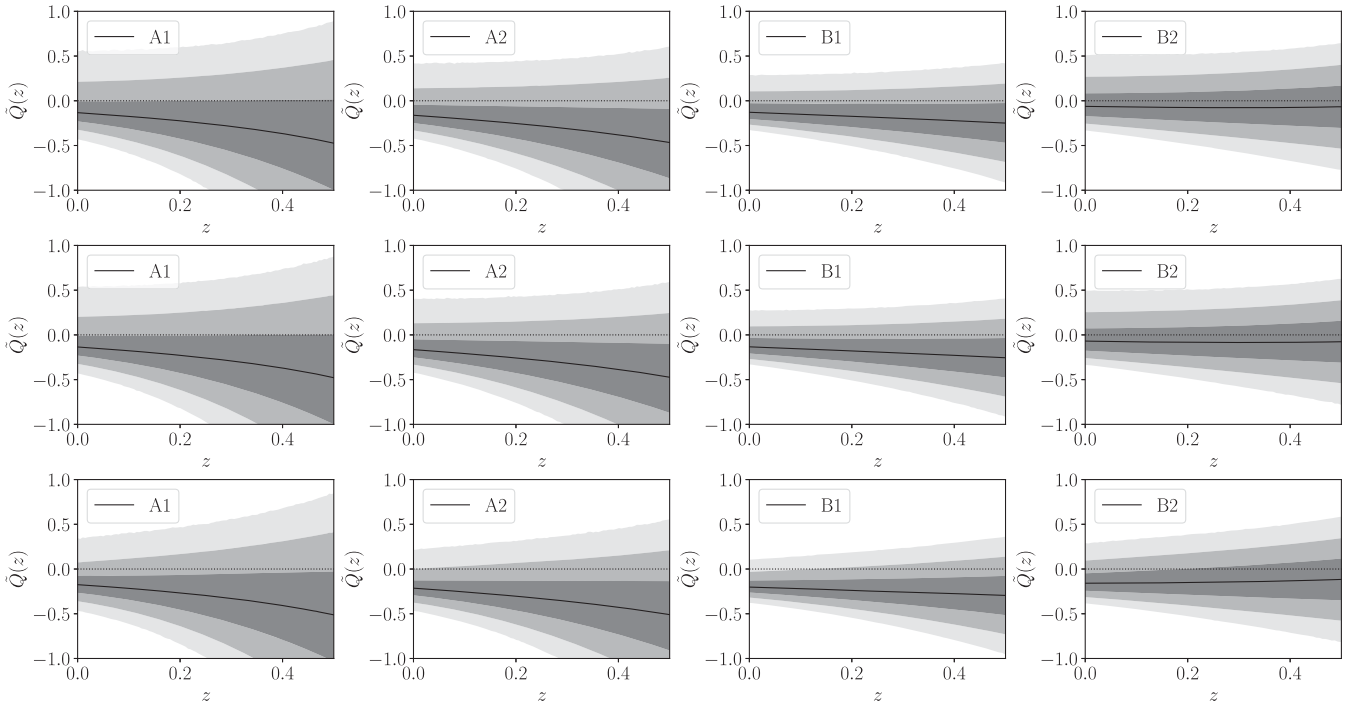

FIG. 3. Plots for the reconstructed $\tilde{Q}$ function in the low redshift range $0 < z < 0.5$ from the data set samples of Sets A and B using a squared exponential covariance function considering the decaying dark energy EoS given by $w = -1$ (top row), the wCDM model with DE EoS given by $w = -1.006 \pm 0.045$ [103] (middle row), and the CPL parametrization of dark energy with DE EoS given by $w(z) = w_0 + w_a(\frac{z}{1+z})$, $w_0 = -1.046^{+0.179}_{-0.170}$, and $w_a = 0.14^{+0.60}_{-0.76}$ [104] (bottom row). The black solid curve shows the best-fit values and the shaded regions correspond to the 1σ, 2σ, and 3σ uncertainties.

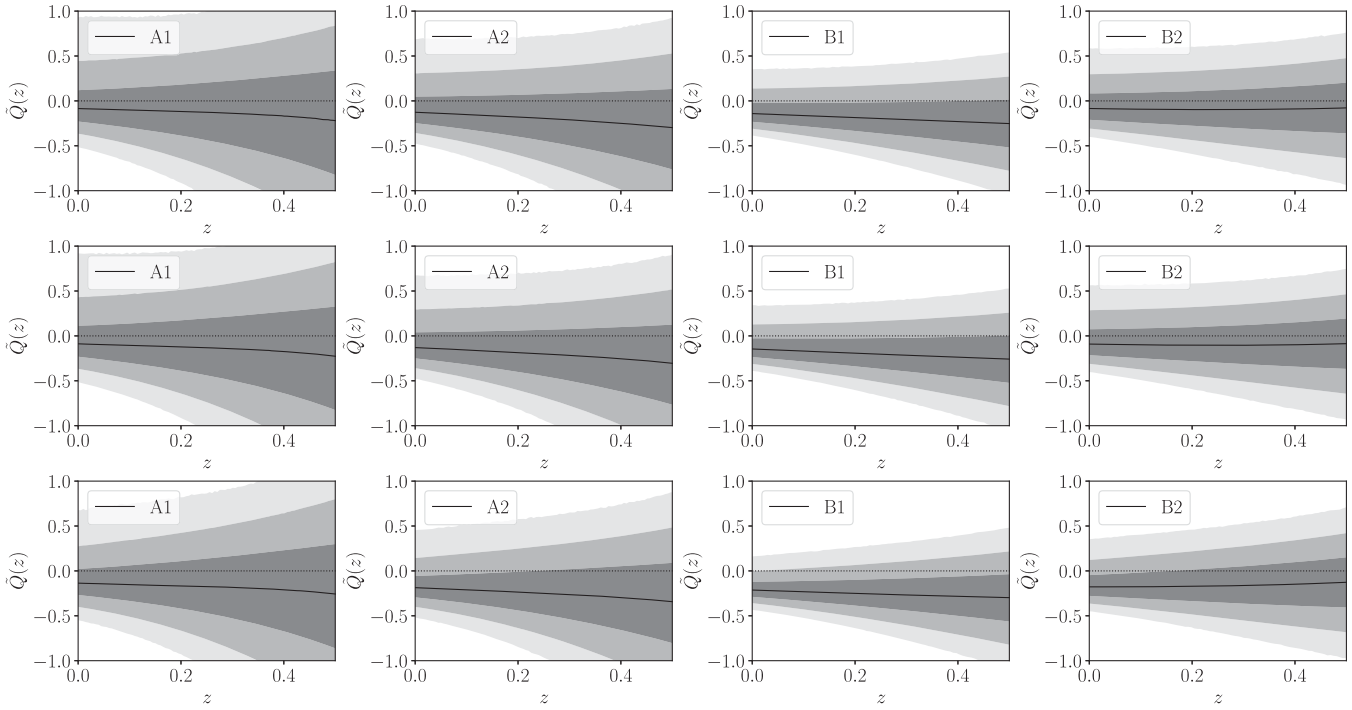

FIG. 4. Plots for the reconstructed $\tilde{Q}$ function in the low redshift range $0 < z < 0.5$ from the data set samples of Sets A and B using a Matérn 9/2 covariance function considering the decaying dark energy EoS given by $w = -1$ (top row), the wCDM model with DE EoS given by $w = -1.006 \pm 0.045$ [103] (middle row), and the CPL parametrization of dark energy with EoS given by $w(z) = w_0 + w_a(\frac{z}{1+z})$, $w_0 = -1.046^{+0.179}_{-0.170}$, and $w_a = 0.14^{+0.60}_{-0.76}$ [104] (bottom row). The black solid curve shows the best-fit values and the shaded regions correspond to the 1σ, 2σ, and 3σ uncertainties.

$$= -0.173 - 0.336\, z \quad \text{for CPL.} \tag{47}$$

For the A2 data set, in the redshift range $0.6 < z < 1$,

$$\tilde{Q}_{\rm fit}(z) = 0.031 - 0.992\, z^2 \quad \text{for } w = -1, \tag{48}$$

$$= 0.025 - 0.993\, z^2 \quad \text{for } w\text{CDM}, \tag{49}$$

$$= -0.011 - 0.973\, z^2 \quad \text{for CPL.} \tag{50}$$

For the B1 data set, in the redshift range $0 < z < 1$,

$$\tilde{Q}_{\rm fit}(z) = -0.121 - 0.291\, z \quad \text{for } w = -1, \tag{51}$$

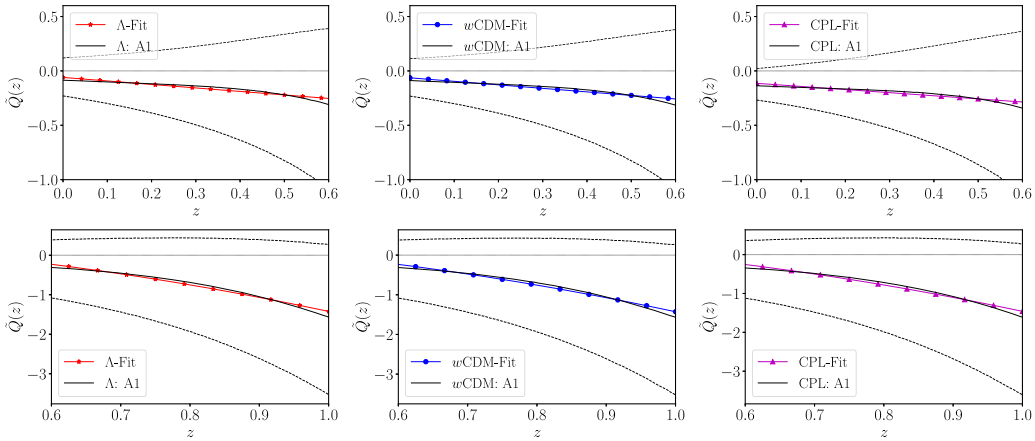

FIG. 5. Plots showing a comparison between the reconstructed interaction $\tilde{Q}(z)$ and the estimated $\tilde{Q}_{\rm fit}(z)$ using the combined data set A1, for EoS given by $w = -1$ (left), wCDM model (middle), and the CPL parametrization (right). The black solid line is the reconstructed function. The line with the marker represents the best-fit result from χ^2 minimization. The 1σ C.L.s are shown as dashed lines.

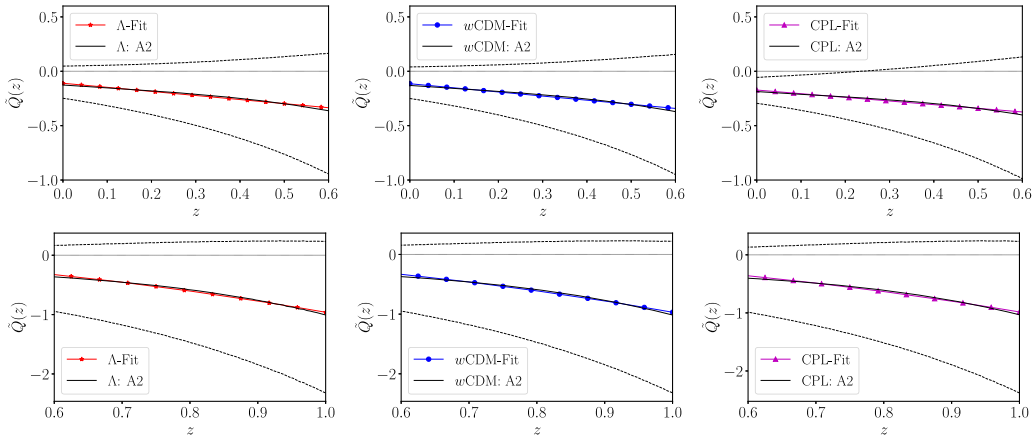

FIG. 6. Plots showing a comparison between the reconstructed interaction $\tilde{Q}(z)$ and the estimated $\tilde{Q}_{\rm fit}(z)$ using the combined data set A2, for EoS given by $w=-1$ (left), wCDM model (middle), and the CPL parametrization (right). The black solid line is the reconstructed function. The line with the marker represents the best-fit result from χ^2 minimization. The 1σ C.L.s are shown as dashed lines.

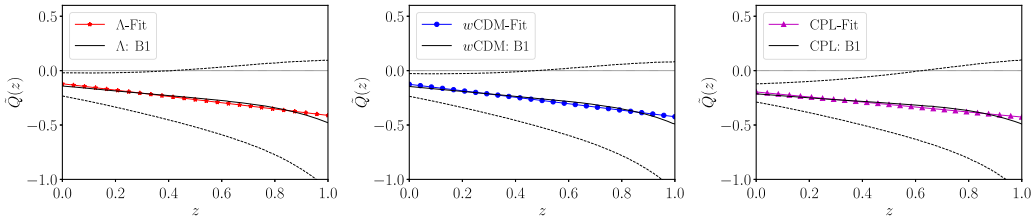

FIG. 7. Plots showing a comparison between the reconstructed interaction $\tilde{Q}(z)$ and the estimated $\tilde{Q}_{\rm fit}(z)$ using the combined data set B1, for EoS given by $w=-1$ (left), wCDM model (middle), and the CPL parametrization (right). The black solid line is the reconstructed function. The line with the marker represents the best-fit result from χ^2 minimization. The 1σ C.L.s are shown as dashed lines.

$$= -0.126 - 0.298\,z \quad \text{for } w\text{CDM}, \tag{52}$$

$$= -0.196 - 0.231\,z \quad \text{for CPL}. \tag{53}$$

For the B2 data set, in the redshift range $0 < z < 1$,

$$\tilde{Q}_{\rm fit}(z) = -0.122 + 0.131\,z \quad \text{for } w=-1, \tag{54}$$

$$= -0.128 + 0.124\,z \quad \text{for } w\text{CDM}, \tag{55}$$

$$= -0.217 - 0.225\,z \quad \text{for CPL}. \tag{56}$$

If we proceed to fitting with any higher-order polynomial, the fitted function will not be contained within the 1σ error margin of $\tilde{Q}(z)$ reconstructed by GP.

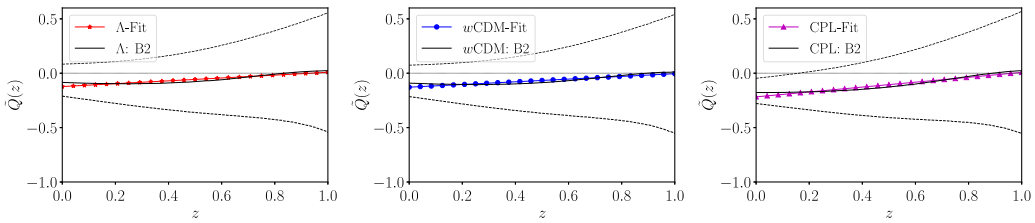

FIG. 8. Plots showing a comparison between the reconstructed interaction $\tilde{Q}(z)$ and the estimated $\tilde{Q}_{\rm fit}(z)$ using the combined data set B2, for EoS given by $w=-1$ (left), wCDM model (middle), and the CPL parametrization (right). The black solid line is the reconstructed function. The line with the markers represents the best-fit result from χ^2 minimization. The 1σ C.L.s are shown as dashed lines.

TABLE VIII. $\tilde{Q}_i$ for best-fit $\tilde{Q}_{\rm fit} = \tilde{Q}_0 + \tilde{Q}_1 z$ in the redshift range $0 < z < 0.6$ and $\tilde{Q}_{\rm fit} = \tilde{Q}_0 + \tilde{Q}_2 z^2$ in the redshift range $0.6 < z < 1$ for data sets A1 and A2.

EoS	Data sets	$\tilde{Q}_0$	$\tilde{Q}_1$	Data sets	$\tilde{Q}_0$	$\tilde{Q}_2$
$w=-1$	A1 $(0<z<0.6)$	$-0.060^{+0.180}_{-0.180}$	$-0.322^{+0.516}_{-0.514}$	A1 $(0.6<z<1)$	$0.443^{+0.329}_{-0.383}$	$-1.865^{+0.558}_{-0.481}$
wCDM	A1 $(0<z<0.6)$	$-0.063^{+0.180}_{-0.180}$	$-0.324^{+0.516}_{-0.516}$	A1 $(0.6<z<1)$	$0.438^{+0.332}_{-0.383}$	$-1.866^{+0.558}_{-0.484}$
CPL	A1 $(0<z<0.6)$	$-0.114^{+0.180}_{-0.180}$	$-0.286^{+0.515}_{-0.518}$	A1 $(0.6<z<1)$	$0.434^{+0.336}_{-0.385}$	$-1.883^{+0.561}_{-0.491}$
$w=-1$	A2 $(0<z<0.6)$	$-0.110^{+0.180}_{-0.180}$	$-0.375^{+0.517}_{-0.516}$	A2 $(0.6<z<1)$	$0.031^{+0.400}_{-0.401}$	$-0.992^{+0.586}_{-0.583}$
wCDM	A2 $(0<z<0.6)$	$-0.115^{+0.179}_{-0.180}$	$-0.379^{+0.517}_{-0.516}$	A2 $(0.6<z<1)$	$0.025^{+0.401}_{-0.401}$	$-0.993^{+0.586}_{-0.583}$
CPL	A2 $(0<z<0.6)$	$-0.173^{+0.180}_{-0.179}$	$-0.336^{+0.517}_{-0.517}$	A2 $(0.6<z<1)$	$-0.011^{+0.401}_{-0.400}$	$-0.973^{+0.582}_{-0.584}$

TABLE IX. $\tilde{Q}_i$ for best-fit $\tilde{Q}_{\rm fit} = \tilde{Q}_0 + \tilde{Q}_1 z$ in the redshift range $0 < z < 1$ for data sets B1 and B2.

EoS	Data sets	$\tilde{Q}_0$	$\tilde{Q}_1$	Data sets	$\tilde{Q}_0$	$\tilde{Q}_1$
$w=-1$	B1 $(0<z<1)$	$-0.121^{+0.153}_{-0.153}$	$-0.291^{+0.262}_{-0.263}$	B2 $(0<z<1)$	$-0.122^{+0.153}_{-0.153}$	$0.131^{+0.263}_{-0.263}$
wCDM	B1 $(0<z<1)$	$-0.126^{+0.152}_{-0.153}$	$-0.298^{+0.264}_{-0.262}$	B2 $(0<z<1)$	$-0.128^{+0.153}_{-0.153}$	$0.124^{+0.264}_{-0.263}$
CPL	B1 $(0<z<1)$	$-0.196^{+0.153}_{-0.153}$	$-0.231^{+0.263}_{-0.263}$	B2 $(0<z<1)$	$-0.217^{+0.153}_{-0.153}$	$0.225^{+0.263}_{-0.263}$

V. EVOLUTION OF THE COSMOLOGICAL DENSITY PARAMETERS

With the nature of the interaction function reconstructed, one can obtain the evolution of energy density parameters as well. The model is a spatially flat, homogenous, and isotropic universe where the total energy density is composed of only a pressureless matter and dark energy. We define the density parameters Ω_i as

$$\Omega_m = \frac{\tilde{\rho}_m}{E^2}, \tag{57}$$

$$\Omega_D = \frac{\tilde{\rho}_D}{E^2}, \tag{58}$$

such that $\Omega_m + \Omega_D = 1$.

We make use of Eq. (14) and rewrite it as

$$\frac{d\tilde{\rho}_m}{dz} - \frac{3\tilde{\rho}_m}{1+z} = \frac{\tilde{Q}}{E(1+z)}. \tag{59}$$

One can see that Eq. (59) is a linear first-order nonhomogeneous differential equation of the form

$$\frac{dy}{dz} + A(z)y = B(z), \tag{60}$$

with $A(z) = -\frac{3}{1+z}$ and $B(z) = \frac{\tilde{Q}}{E(1+z)}$. The integrating factor for Eq. (60) is given by $e^{\int A(z)dz}$, and the general solution is

$$y = e^{-\int A dz}\int (Be^{\int A dz})dz + C, \tag{61}$$

where C is the constant of integration.

Similarly, we solve for Eq. (59) and arrive at an expression for the reduced matter density $\tilde{\rho}_m$,

$$\tilde{\rho}_m = \tilde{\rho}_{m0}(1+z)^3 + (1+z)^3\int_0^z \frac{\tilde{Q}}{E}(1+z)^{-4}dz. \tag{62}$$

If $\tilde{Q} = 0$, Eq. (62) reduces to the relation $\tilde{\rho}_m = \tilde{\rho}_{m0}(1+z)^3$ [where $\tilde{\rho}_{m0} = \tilde{\rho}_m(z=0)$] which is the standard evolution scenario for a pressureless matter that evolves independently. One can now write the density parameters with the help of Eqs. (57)–(58) as

$$\Omega_m = \frac{\tilde{\rho}_{m0}(1+z)^3}{E^2} + \frac{(1+z)^3}{E^2}\int_0^z \frac{\tilde{Q}}{E(1+z)^4}dz, \tag{63}$$

$$\Omega_D = 1 - \Omega_m. \tag{64}$$

With the smooth functions of $E(z)$ and $\tilde{Q}(z)$ reconstructed from the combined data sets, we use the trapezoidal rule [107] to calculate the integral

$$\begin{aligned} f(z) &= \int_0^z \frac{\tilde{Q}}{E}(1+z)^{-4}dz \\ &= \int_0^z g(z)dz \\ &\simeq \frac{1}{2}\sum_{i=0}^{n}(z_{i+1}-z_i)[g(z_{i+1}) + g(z_i)], \end{aligned} \tag{65}$$

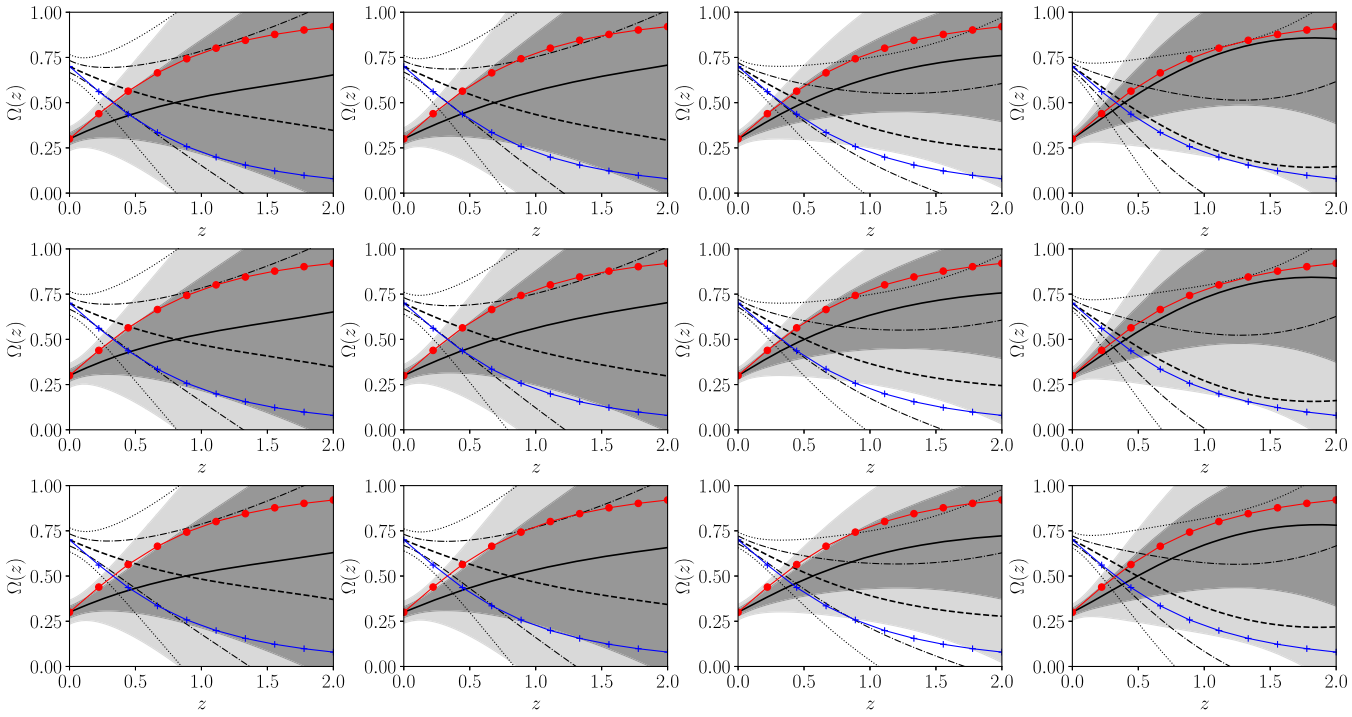

FIG. 9. Plots for the dark energy density Ω_D and the matter density Ω_m from the data set samples of Set A1 (column 1), Set A2 (column 2), Set B1 (column 3), and Set B2 (column 4) using a squared exponential covariance function considering the decaying dark energy EoS given by $w = -1$ (top row), the wCDM model with DE EoS given by $w = -1.006 \pm 0.045$ [103] (middle row), and the CPL parametrization of dark energy with EoS given by $w(z) = w_0 + w_a(\frac{z}{1+z})$, $w_0 = -1.046^{+0.179}_{-0.170}$, and $w_a = 0.14^{+0.60}_{-0.76}$ [104] (bottom row). The black solid curve corresponds to Ω_m while the black dashed line represents Ω_D. The 1σ and 2σ uncertainties in Ω_m are shown by the dark and light shaded regions, and those of Ω_D are given by the regions bounded with dashed-dotted and dotted lines, respectively. The line drawn with circles represents Ω_m and the line with cross markers is that of Ω_D, for the ΛCDM model.

where $g(z) = \frac{\tilde{Q}}{E}(1+z)^{-4}$. The uncertainty in $f(z)$ is obtained using the error propagation formula,

$$\sigma_f^2 = \frac{1}{4}\sum_{i=0}^{n}(z_{i+1} - z_i)^2[\sigma_{g_{i+1}}^2 + \sigma_{g_i}^2], \tag{66}$$

where the contributions from the uncertainties in $\tilde{Q}$ and E have been included.

We plot the density parameters Ω_m and Ω_D using Eqs. (57) and (58). We choose the value $\tilde{\rho}_{m0} = 0.3$, i.e., $\Omega_{m0} = \frac{0.3}{E(0)^2}$. The plots are shown in Figs. 9 and 10 for the two choices of the covariance function.

For the three different choices of the interacting dark energy models, the evolutions of the density parameters are found to be qualitatively similar and also not too sensitive to the choice of the data sets. This feature hardly depends on the choice of the covariance function, except for the fact that the use of the Matérn 9/2 covariance function brings the transition to dark energy dominance a bit closer to $z = 0.5$. One intriguing common feature to note is that for the interacting models, Ω_D takes over as the dominant role over Ω_m later in the evolution (closer to $z = 0$) compared to the corresponding ΛCDM model.

One can note that the transition from a matter-dominated phase to a dark-energy-dominated phase occurs within the redshift range $0.5 < z < 1$.

VI. THERMODYNAMICS OF THE INTERACTION

For the thermodynamic properties of the model, we consider the universe as a system that is bounded by some cosmological horizon, and the matter content of the universe is enclosed within a volume defined by a radius not bigger than the horizon. It is worth mentioning that this idea primarily originated from the consideration of black hole thermodynamics, which is equally valid for a cosmological horizon [3,108,109]. However, in an evolving scenario such as in cosmology, an apparent horizon is more relevant than an event horizon. An apparent horizon is given by the equation $g^{\mu\nu}R_{,\mu}R_{,\nu} = 0$. For a spatially flat FLRW universe, this equation tells us that the apparent horizon (r_h) is in fact the Hubble horizon,

$$r_h = \frac{1}{H}. \tag{67}$$

This serves the purpose of recovering the first law of thermodynamics. For a comprehensive description, we

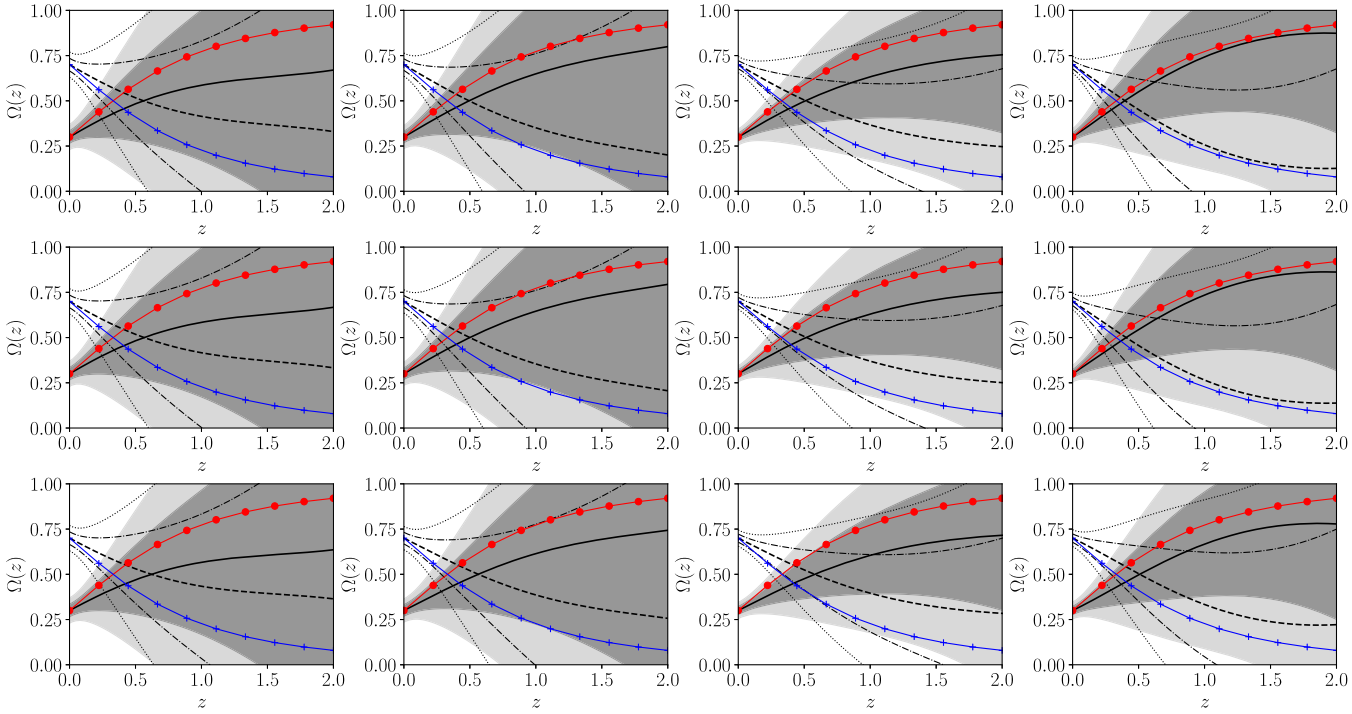

FIG. 10. Plots for the dark energy density Ω_D and the matter density Ω_m from the data set samples of Set A1 (column 1), Set A2 (column 2), Set B1 (column 3), and Set B2 (column 4) using a Matérn 9/2 covariance function considering the decaying dark energy EoS given by $w=-1$ (top row), the wCDM model with DE EoS given by $w=-1.006\pm0.045$ [103] (middle row), and the CPL parametrization of dark energy with EoS given by $w(z)=w_0+w_a(\frac{z}{1+z})$, $w_0=-1.046^{+0.179}_{-0.170}$, and $w_a=0.14^{+0.60}_{-0.76}$ [104] (bottom row). The black solid curve corresponds to Ω_m while the black dashed line represents Ω_D. The 1σ and 2σ uncertainties in Ω_m are shown by the dark and light shaded regions, and those of Ω_D are given by the regions bounded with dashed-dotted and dotted lines, respectively. The line drawn with circles represents Ω_m and the line with cross markers is that of Ω_D, for the ΛCDM model.

refer to the work of Ferreira and Pavón [110] and the monograph by Faraoni [111].

For the second law to be valid, the entropy S should be nondecreasing with respect to the expansion of the universe. If S_f and S_h stand for the entropy of the fluid and that of the horizon containing the fluid, respectively, then the total entropy of the system, i.e., $S=S_f+S_h$, should satisfy the relation

$$\frac{dS}{dx}\geq 0, \tag{68}$$

where $x=\ln a$, with a being the scale factor of the universe. For an approach to equilibrium, the condition is

$$\frac{d^2S}{dx^2}<0. \tag{69}$$

With the apparent horizon as the cosmological horizon, the entropy of the horizon S_h can be written as [112]

$$S_h=8\pi^2r_h^2=\frac{8\pi^2}{H^2}. \tag{70}$$

Further, the temperature of the dynamical apparent horizon is related to the horizon radius by the relation

$$T_h=\frac{1}{2\pi r_h}\left[1-\frac{\dot{r_h}}{2Hr_h}\right]=\frac{2H^2+\dot{H}}{4\pi H}, \tag{71}$$

which is called the Hayward-Kodama temperature [113,114]. As the cosmological horizon is evolving, the Hawking temperature is replaced by Hayward-Kodama temperature (see Ref. [111]).

Now, if we denote $S_f=S_m+S_D$, where S_m and S_D are the entropies of the matter sector and dark energy sector, with T being the temperature of the composite matter distribution inside the horizon, then the first law of thermodynamics $TdS=dE+pdV$ can be recast for the individual matter components in the following form:

$$TdS_m=dE_m+p_mdV=dE_m, \tag{72}$$

$$TdS_D=dE_D+p_DdV, \tag{73}$$

where $V=\frac{4}{3}\pi r_h^3=\frac{4\pi}{3H^2}$ is the fluid volume. E_m and E_D represent the internal energies of the dark matter and energy components, given by $E_m=\frac{4}{3}\pi r_h^3\rho_m=\rho_mV$ and $E_D=\frac{4}{3}\pi r_h^3\rho_D=\rho_DV$, respectively. Now, differentiating Eqs. (70), (72), and (73) with respect to cosmic time t along

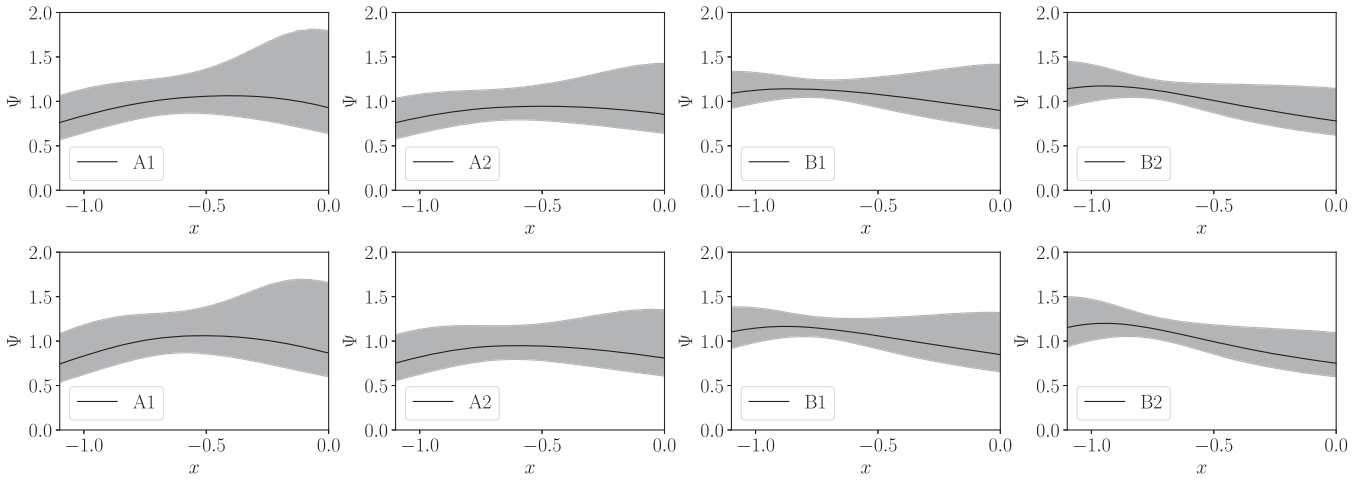

FIG. 11. Plots for Ψ from the data set samples of Sets A and B using a squared exponential covariance (top row) and the Matérn 9/2 covariance function. The solid black line gives the best-fit values of Ψ. The shaded region corresponds to the 1σ uncertainty.

with the assumption that T should be equal to T_h [Eq. (71)], we get

$$\dot{S_m} + \dot{S_D} = 16\pi^2 \frac{\dot{H}}{H^3}\left(1 + \frac{\dot{H}}{2H^2 + \dot{H}}\right), \tag{74}$$

$$\dot{S_h} = -16\pi^2 \frac{\dot{H}}{H^3}. \tag{75}$$

Therefore,

$$\dot{S} = \dot{S_m} + \dot{S_D} + \dot{S_h} = 16\pi^2 \frac{\dot{H}^2}{H^3}\left(\frac{1}{2H^2 + \dot{H}}\right). \tag{76}$$

One should note that it may not always be justified to assume that the fluid temperature is equal to the horizon temperature. This assumption is particularly unjustified for a radiation distribution that obeys Stefan's law. However, for pressureless matter the equality of T and T_h is valid, and for dark energy this equality is at least approximately correct. Thus, in the present context, this assumption is not at all drastic. For an account of this justification, we refer to the work of Mimoso and Pavón [115].

The relation (76) can be written with x as the argument, where $x = \ln a = -\ln(1+z)$, as

$$\frac{dS}{dx} = \frac{16\pi^2}{H^4}\left(\frac{dH}{dx}\right)^2 \Psi(x), \tag{77}$$

where

$$\Psi(x) = \left[2 + \frac{1}{H}\frac{dH}{dx}\right]^{-1}. \tag{78}$$

Again, upon differentiating Eq. (77) with respect to x, one obtains

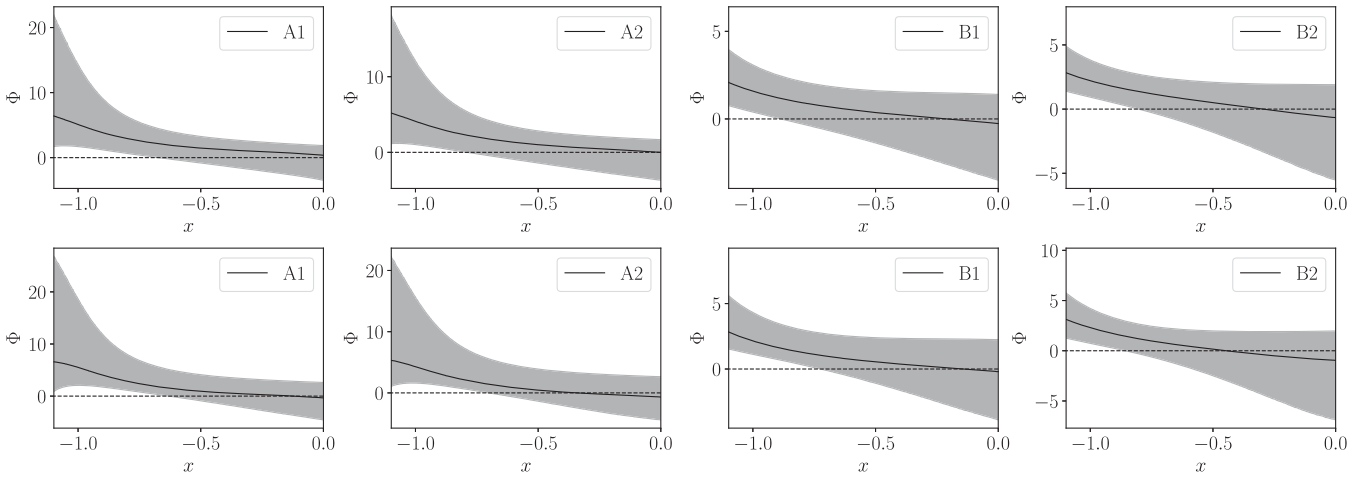

FIG. 12. Plots for Φ from the data set samples of Sets A and B using a squared exponential covariance (top row) and the Matérn 9/2 covariance function. The solid black line gives the best-fit values of Φ. The shaded region corresponds to the 1σ uncertainty.

$$\frac{d^2S}{dx^2} = \frac{16\pi^2\Psi^2}{H^4}\left(\frac{dH}{dx}\right)^2\Phi(x), \tag{79}$$

where

$$\Phi = \left[\frac{1}{H}\frac{d^2H}{dx^2} - \frac{3}{H^2}\left(\frac{dH}{dx}\right)^2 + \frac{4}{\frac{dH}{dx}}\frac{d^2H}{dx^2} - \frac{8}{H}\frac{dH}{dx}\right]. \tag{80}$$

From Eq. (77) we see that for the inequality (68) to hold true, the required condition is $\Psi \geq 0$. Equation (79) shows that the condition (69) will be satisfied provided that $\Phi < 0$. We try to understand the behavior of Ψ and Φ by plotting them in Figs. 11 and 12, respectively, as functions of x, where $x = -\ln(1+z)$.

The plots in Fig. 11 show that Ψ remains positive at 1σ throughout the domain of reconstruction $0 < z < 2$. Thus, the second law of thermodynamics is indeed satisfied for the reconstructed scenario. From Fig. 12 the plots reveal that Φ was positive in the past, but as we approach the present epoch the value of Φ decreases gradually and changes its signature. The best-fit value Φ becomes negative as x increases. This hints towards a possibility that the universe is undergoing a change from a thermodynamic nonequilibrium in the past towards an equilibrium state in the present epoch.

VII. DISCUSSION

It is argued quite often that the possibility of a nongravitational interaction in the cosmic dark sector should not be ruled out *a priori*. As the nature of dark energy is not known, it is impossible to model the interaction theoretically. The normal practice is to assume a transfer of energy between dark matter and dark energy and write the rate of transfer Q as a function of the densities ρ_D or ρ_m, or both, and even their derivatives [116], and thus parametrize Q. The next step is to reconstruct the model parameters using the observational data. This is indeed biased in a way, as the functional form of Q is already chosen.

The present work employed the widely practiced Gaussian process and made an attempt to reconstruct the transfer of energy Q in a dimensionless representation (defined as $\tilde{Q} = \frac{Q}{3H_0^2}$) directly from observational data sets without any parametrization. Thus, no functional form of Q was assumed. Various combinations of data sets were utilized, properly described in Sec. III. There have been only a few investigations on a nonparametric reconstruction of Q, as mentioned in the Introduction. The primary difference between the present work and the existing literature is that we used more recent data sets and investigated three different versions of dark energy. They are (i) an interacting vacuum with $w = -1$, (ii) a wCDM model where w is close to but not exactly equal to -1, and (iii) the CPL parametrization where $w(z) = w_0 + w_a\frac{z}{1+z}$. The universal feature that we found is that for any of these choices and any combination of data sets, an interaction in the dark sector is not significant at the present epoch. The interaction may not be ruled out in the past, beyond $z \geq 0.5$, but a zero Q is indeed a possibility normally in 2σ and at most in 3σ. This result is different from the oscillatory behavior, as noted by Cai and Su [18]. Our result is closer to that given by Wang *et al.* [62] where a nonparametric Bayesian approach indicated that an interacting vacuum is not preferred.

An analytic expression for the energy transfer rate Q in the form of a polynomial in z was given in Sec. IV. The reduced χ^2 test allowed up to second order in z for some combinations (A1 and A2) and only up to first order in z for the other two combinations (B1 and B2) of data sets.

The evolution of the density parameters Ω_m and Ω_D were also checked in the presence of the interaction in the dark sector. The common feature that arose was that the dominance of dark energy is delayed a bit (closer to $z = 0$).

The thermodynamic considerations reveal an interesting possibility. While the reconstructed interaction does not infringe upon the thermodynamic viability in terms of the increase in entropy, the universe seems to be evolving towards a thermodynamic equilibrium only from the recent past, namely, $x \sim -0.5$, i.e., close to $z \sim 0.6$.

ACKNOWLEDGMENTS

P. M. thanks her colleagues for lively discussions.

[1] A. G. Riess *et al.* (Supernova Search Team Collaboration), Astron. J. **116**, 1009 (1998).
[2] S. Perlmutter *et al.* (Supernova Cosmology Project Collaboration), Astrophys. J. **517**, 565 (1999).
[3] T. Padmanabhan, Phys. Rep. **380**, 235 (2003).
[4] P. J. E. Peebles and B. Ratra, Rev. Mod. Phys. **75**, 559 (2003).
[5] S. Weinberg, Rev. Mod. Phys. **61**, 1 (1989).
[6] P. Brax, Rep. Prog. Phys. **81**, 016902 (2018).
[7] E. J. Copeland, M. Sami, and S. Tsujikawa, Int. J. Mod. Phys. D **15**, 1753 (2006).
[8] V. Sahni and A. Starobinsky, Int. J. Mod. Phys. D **15**, 2105 (2006).
[9] I. Zlatev, L. Wang, and P. J. Steinhardt, Phys. Rev. Lett. **82**, 896 (1999).
[10] R. N. Henriksen, Phys. Lett. **119B**, 85 (1982).
[11] T. Olson and T. F. Jordan, Phys. Rev. D **35**, 3258 (1987).

[12] G. R. Farrar and P. J. E. Peebles, Astrophys. J. **604**, 1 (2004).
[13] R.-G. Cai and A. Wang, J. Cosmol. Astropart. Phys. 03 (2005) 002.
[14] L. Amendola, G. C. Campos, and R. Rosenfeld, Phys. Rev. D **75**, 083506 (2007).
[15] Z.-K. Guo, N. Ohta, and S. Tsujikawa, Phys. Rev. D **76**, 023508 (2007).
[16] J. H. He and B. Wang, J. Cosmol. Astropart. Phys. 06 (2008) 010.
[17] G. Caldera-Cabral, R. Maartens, and L. A. Urena-Lopez, Phys. Rev. D **79**, 063518 (2009).
[18] R.-G. Cai and Q. Su, Phys. Rev. D **81**, 103514 (2010).
[19] L. L. Honorez, B. A. Reid, O. Mena, L. Verde, and R. Jimenez, J. Cosmol. Astropart. Phys. 09 (2010) 029.
[20] D. Bessada and O. D. Miranda, Phys. Rev. D **88**, 083530 (2013).
[21] W. Yang and L. Xu, Phys. Rev. D **89**, 083517 (2014).
[22] A. Paliathanasis and M. Tsamparlis, Phys. Rev. D **90**, 043529 (2014).
[23] D. G. A. Duniya, D. Bertacca, and R. Maartens, Phys. Rev. D **91**, 063530 (2015).
[24] J. Valiviita and E. Palmgren, J. Cosmol. Astropart. Phys. 07 (2015) 015.
[25] S. del Campo, R. Herrera, and D. Pavn, Phys. Rev. D **91**, 123539 (2015).
[26] A. Mukherjee, J. Cosmol. Astropart. Phys. 11 (2016) 055.
[27] S. Pan and G. S. Sharov, Mon. Not. R. Astron. Soc. **472**, 4736 (2017).
[28] A. Mukherjee and N. Banerjee, Classical Quantum Gravity **34**, 035016 (2017).
[29] S. Pan, A. Mukherjee, and N. Banerjee, Mon. Not. R. Astron. Soc. **477**, 1189 (2018).
[30] P. Mukherjee, A. Mukherjee, H. K. Jassal, A. Dasgupta, and N. Banerjee, Eur. Phys. J. Plus **134**, 147 (2019).
[31] G. S. Sharov, S. Bhattacharya, S. Pan, R. C. Nunes, and S. Chakraborty, Mon. Not. R. Astron. Soc. **466**, 3497 (2017).
[32] S. D. Odintsov, V. K. Oikonomou, and P. V. Tretyakov, Phys. Rev. D **96**, 044022 (2017).
[33] W. Yang, N. Banerjee, and S. Pan, Phys. Rev. D **95**, 123527 (2017).
[34] E. Di Valentino, A. Melchiorri, and O. Mena, Phys. Rev. D **96**, 043503 (2017).
[35] W. Yang, S. Pan, and J. D. Barrow, Phys. Rev. D **97**, 043529 (2018).
[36] W. Yang, S. Pan, and D. F. Mota, Phys. Rev. D **96**, 123508 (2017).
[37] V. Salvatelli, N. Said, M. Bruni, A. Melchiorri, and D. Wands, Phys. Rev. Lett. **113**, 181301 (2014).
[38] W. Yang and L. Xu, Phys. Rev. D **90**, 083532 (2014).
[39] W. Yang and L. Xu, J. Cosmol. Astropart. Phys. 08 (2014) 034.
[40] R. C. Nunes, S. Pan, and E. N. Saridakis, Phys. Rev. D **94**, 023508 (2016).
[41] S. Kumar and R. C. Nunes, Phys. Rev. D **94**, 123511 (2016).
[42] W. Yang, H. Li, Y. Wu, and J. Lu, J. Cosmol. Astropart. Phys. 10 (2016) 007.
[43] A. Pourtsidou and T. Tram, Phys. Rev. D **94**, 043518 (2016).
[44] B. Wang, E. Abdalla, F. Atrio-Barandela, and D. Pavón, Rep. Prog. Phys. **79**, 096901 (2016).
[45] M. Sahlén, A. R. Liddle, and D. Parkinson, Phys. Rev. D **72**, 083511 (2005).
[46] M. Sahlén, A. R. Liddle, and D. Parkinson, Phys. Rev. D **75**, 023502 (2007).
[47] T. Holsclaw, U. Alam, B. Sansó, H. Lee, K. Heitmann, S. Habib, and D. Higdon, Phys. Rev. D **82**, 103502 (2010).
[48] T. Holsclaw, U. Alam, B. Sansó, H. Lee, K. Heitmann, S. Habib, and D. Higdon, Phys. Rev. Lett. **105**, 241302 (2010).
[49] T. Holsclaw, U. Alam, B. Sansó, H. Lee, K. Heitmann, S. Habib, and D. Higdon, Phys. Rev. D **84**, 083501 (2011).
[50] R. G. Crittenden, G. B. Zhao, L. Pogosian, L. Samushia, and X. Zhang, J. Cosmol. Astropart. Phys. 02 (2012) 048.
[51] R. Nair, S. Jhingan, and D. Jain, J. Cosmol. Astropart. Phys. 01 (2014) 005.
[52] Z. Zhang, G. Gu, X. Wang, Y.-H. Li, C. G. Sabiu, H. Park, H. Miao, X. Luo, F. Fang, and X.-D. Li, Astron. J. **878**, 137 (2019).
[53] M. Bilicki and M. Seikel, Mon. Not. R. Astron. Soc. **425**, 1664 (2012).
[54] H.-N. Lin, X. Li, and L. Tang, Chin. Phys. C **43**, 075101 (2019).
[55] M.-J. Zhang and J.-Q. Xia, J. Cosmol. Astropart. Phys. 12 (2016) 005.
[56] R. C. Nunes, S. K. Yadav, J. F. Jesus, and A. Bernui, Mon. Not. R. Astron. Soc. **497**, 2133 (2020).
[57] C. A. P. Bengaly, Mon. Not. R. Astron. Soc. **499**, L6 (2020).
[58] J. F. Jesus, R. Valentim, A. A. Escobal, and S. H. Pereira, J. Cosmol. Astropart. Phys. 04 (2020) 053.
[59] R. Arjona and S. Nesseris, Phys. Rev. D **101**, 123525 (2020).
[60] P. Mukherjee and N. Banerjee, arXiv:2007.15941.
[61] P. Mukherjee and N. Banerjee, Eur. Phys. J. C **81**, 36 (2021).
[62] Y. Wang, G. B. Zhao, D. Wands, L. Pogosian, and R. G. Crittenden, Phys. Rev. D **92**, 103005 (2015).
[63] T. Yang, Z.-K. Guo, and R.-G. Cai, Phys. Rev. D **91**, 123533 (2015).
[64] R.-G. Cai, N. Tamaninic, and T. Yang, J. Cosmol. Astropart. Phys. 05 (2017) 031.
[65] M. Chevallier and D. Polarski, Int. J. Mod. Phys. **D10**, 213 (2001).
[66] C. Rasmussen and C. Williams, *Gaussian Processes for Machine Learning* (The MIT Press, Cambridge, MA, 2006).
[67] D. MacKay, *Information Theory, Inference and Learning Algorithms* (Cambridge University Press, Cambridge, England, 2003), Chap. 45.
[68] C. Williams, Prediction with Gaussian processes: From linear regression to linear prediction and beyond, in *Learning in Graphical Models*, edited by M. I. Jordan (The MIT Press, Cambridge, MA, 1999), pp. 599–621.
[69] M. Seikel, C. Clarkson, and M. Smith, J. Cosmol. Astropart. Phys. 06 (2012) 036.
[70] A. Shafieloo, A. G. Kim, and E. V. Linder, Phys. Rev. D **85**, 123530 (2012).

[71] S. Yahya, M. Seikel, C. Clarkson, R. Maartens, and M. Smith, Phys. Rev. D **89**, 023503 (2014).
[72] S. Santos-da Costa, V. C. Busti, and R. F. Holanda, J. Cosmol. Astropart. Phys. 10 (2015) 061.
[73] R.-G. Cai, Z.-K. Guo, and T. Yang, Phys. Rev. D **93**, 043517 (2016).
[74] D. Wang and X.-H. Meng, Phys. Rev. D **95**, 023508 (2017).
[75] D. Wang, W. Zhang, and X.-H. Meng, Eur. Phys. J. C **79**, 211 (2019).
[76] http://www.gaussianprocess.org
[77] M. Seikel and C. Clarkson, arXiv:1311.6678.
[78] https://github.com/carlosandrepaes/GaPP
[79] C. Zhang, H. Zhang, S. Yuan, T.-J. Zhang, and Y.-C. Sun, Res. Astron. Astrophys. **14**, 1221 (2014).
[80] D. Stern, R. Jimenez, L. Verde, M. Kamionkowski, and S. A. Stanford, J. Cosmol. Astropart. Phys. 02 (2010) 008.
[81] M. Moresco *et al.*, J. Cosmol. Astropart. Phys. 08 (2012) 006.
[82] M. Moresco, L. Pozzetti, A. Cimatti, R. Jimenez, C. Maraston, L. Verde, D. Thomas, A. Citro, R. Tojeiro, and D. Wilkinson, J. Cosmol. Astropart. Phys. 05 (2016) 014.
[83] A. L. Ratsimbazafy, S. I. Loubser, S. M. Crawford, C. M. Cress, B. A. Bassett, R. C. Nichol, and P. Visnen, Mon. Not. R. Astron. Soc. **467**, 3239 (2017).
[84] M. Moresco, Mon. Not. R. Astron. Soc. **450**, L16 (2015).
[85] M. Ĺopez-Corredoira, A. Vazdekis, C. M. Gutíerrez, and N. Castro-Rodŕguez, Astron. Astrophys. **600**, A91 (2017).
[86] M. Ĺopez-Corredoira and A. Vazdekis, Astron. Astrophys. **614**, A127 (2018).
[87] M. Moresco, R. Jimenez, L. Verde, L. Pozzetti, A. Cimatti, and A. Citro, Astrophys. J. **868**, 84 (2018).
[88] A. G. Riess *et al.*, Astrophys. J. **853**, 126 (2018).
[89] E. Gaztanaga, A. Cabre, and L. Hui, Mon. Not. R. Astron. Soc. **399**, 1663 (2009).
[90] A. Oka, S. Saito, T. Nishimichi, A. Taruya, and K. Yamamoto, Mon. Not. R. Astron. Soc. **439**, 2515 (2014).
[91] Y. Wang *et al.* (BOSS Collaboration), Mon. Not. R. Astron. Soc. **469**, 3762 (2017).
[92] C.-H. Chuang and Y. Wang, Mon. Not. R. Astron. Soc. **435**, 255 (2013).
[93] S. Alam *et al.* (BOSS Collaboration), Mon. Not. R. Astron. Soc. **470**, 2617 (2017).
[94] C. Blake, S. Brough, M. Colless *et al.*, Mon. Not. R. Astron. Soc. **425**, 405 (2012).
[95] N. G. Busca, T. Delubac, J. Rich *et al.*, Astron. Astrophys. **552**, A96 (2013).
[96] C.-H. Chuang *et al.*, Mon. Not. R. Astron. Soc. **433**, 3559 (2013).
[97] L. Anderson *et al.* (BOSS Collaboration), Mon. Not. R. Astron. Soc. **441**, 24 (2014).
[98] J. E. Bautista *et al.*, Astron. Astrophys. **603**, A12 (2017).
[99] T. Delubac *et al.* (BOSS Collaboration), Astron. Astrophys. **574**, A59 (2015).
[100] A. Font-Ribera *et al.* (BOSS Collaboration), J. Cosmol. Astropart. Phys. 05 (2014) 027.
[101] G.-B. Zhao *et al.*, Mon. Not. R. Astron. Soc. **482**, 3497 (2019).
[102] H. M. Bourboux *et al.*, Astron. Astrophys. **608**, A130 (2017).
[103] P. A. R. Ade *et al.* (Planck Collaboration), Astron. Astrophys. **594**, A13 (2016).
[104] N. Suzuki, D. Rubin, C. Lidman *et al.*, Astrophys. J. **746**, 85 (2012).
[105] D. Pavón and B. Wang, Gen. Relativ. Gravit. **41**, 1 (2009).
[106] L. P. Chimento and D. Pavón, Phys. Rev. D **73**, 063511 (2006).
[107] R. Holanda, J. Carvalho, and J. Alcaniz, J. Cosmol. Astropart. Phys. 04 (2013) 027.
[108] G. W. Gibbons and S. W. Hawking, Phys. Rev. D **15**, 2738 (1977).
[109] T. Jacobson, Phys. Rev. Lett. **75**, 1260 (1995).
[110] P. C. Ferreira and D. Pavón, Eur. Phys. J. C **76**, 37 (2016).
[111] V. Faraoni, *Cosmological and Black Hole Apparent Horizons* (Springer International Publishing, Switzerland, 2015).
[112] D. Bak and S. J. Rey, Classical Quantum Gravity **17**, L83 (2000).
[113] S. A. Hayward, Classical Quantum Gravity **15**, 3147 (1998).
[114] S. A. Hayward, R. Di Criscienzo, L. Vanzo, M. Nadalini, and S. Zerbini, Classical Quantum Gravity **26**, 062001 (2009).
[115] J. P. Mimoso and D. Pavón, Phys. Rev. D **94**, 103507 (2016).
[116] W. Yang, N. Banerjee, A. Paliathanasis, and S. Pan, Phys. Dark Universe **26**, 100383 (2019).